Contact force control in multibody pantograph/catenary systems

Carmine M. Pappalardo[1], Mohil D. Patel[2], Brian Tinsley[2] and Ahmed A. Shabana[2]

[1]Department of Industrial Engineering, University of Salerno, Italy
[2]Department of Mechanical and Industrial Engineering, University of Illinois at Chicago, USA

Corresponding author:
Ahmed A. Shabana, Department of Mechanical and Industrial Engineering, University of Illinois at Chicago, 842 West Taylor Street, Chicago, IL, USA.
Email: shabana@uic.edu

Abstract
In this paper, a new continuum-based pantograph/catenary model based on the *absolute nodal coordinate formulation* (ANCF) is proposed and used to develop an effective method to control the contact force which arises from the pantograph/catenary interaction. In the proposed new model, only one ANCF gradient vector is used in the formulation of the pantograph/catenary contact conditions, thereby allowing for using the proposed approach for both fully parameterized and gradient deficient ANCF finite elements. The proposed contact formulation can also be considered as a more general sliding joint formulation that allows for the use of the more efficient gradient deficient ANCF finite elements in modeling very flexible cables. A three-dimensional multibody system (MBS) model of a pantograph mounted on a train is developed using a nonlinear augmented MBS formulation. In order to take into account the catenary large deformation, ANCF finite elements are used. The contact between the pantograph and the catenary system is ensured using a sliding joint constraint whereas the contact between the rail vehicle wheels and the train track is modelled using an elastic contact formulation. In addition to the use of the new MBS approach to model the pantograph/catenary interaction, the contact force between the pantograph and the catenary is computed using a simpler lumped parameter model which describes the pan-head and the plunger subsystem dynamics. In order to reduce the standard deviation of the contact force without affecting its mean value, a control actuator is used between the pan-head and the plunger. To this end, three types of control laws for the control action are designed to improve the contact quality both in the transient phase and in the steady state phase of the pantograph/catenary interaction. The first control law proposed features a feedback structure whereas the second and the third control strategies employ a feedback plus feed-forward architecture. In order to demonstrate the effectiveness of the proposed method, the results of a set of numerical simulations with and without the controllers are presented.

Keywords
Multibody systems dynamics; absolute nodal coordinate formulation; pantograph/catenary interaction; wheels/rail contact; optimal control; dynamic damping controller

Introduction

Pantograph catenary systems power the world's fastest trains because electricity is the only viable method to power trains at speeds over 300 km/h.[1-3] While operating at such high speeds, maintaining stability in the catenary system as well as in the pantograph system becomes a primary design goal. Control systems can be employed in order to help the system to operate nominally even under harsh operating conditions. In order to design effective control systems, accurate modeling of the dynamics of the system components is required.[4] Therefore, in this investigation the absolute nodal coordinate formulation (ANCF) is used to model the catenary whereas the pantograph is modeled using rigid MBS dynamics.[5] The proper functionality of the current collection system is determined by its dynamic behavior which results from the pantograph/catenary interaction; thus, this must be carefully analyzed.[6] Particularly, the accurate prediction of the time evolution of the contact force between the pantograph strips and the catenary wire has been found to be a key metric in assessing the performance of this form of energy collection system. The variation of the interaction force between the pantograph and the catenary can be due to different factors such as the vibration of the car body or the presence of adverse weather conditions.[7] In the worst-case scenario, these factors can lead to a complete loss of contact or damage of the railway infrastructure. In order to maintain pan-head/catenary contact, the sliding contact between the pantograph strips and the catenary wire is imposed through the action of an uplift force exerted by an actuator on the pantograph lower arm. If the uplift force is too large, a large contact force between the pantograph strips and the catenary wire is generated which can lead to escalated wear of the components in contact due to the large friction force. On the other hand, if the applied uplift force is too weak, the contact force

produced between the pantograph/catenary system is too small, which can lead to a loss of contact, increasing the probability of electrical arcing. Thus, the stability of the electrical contact is the most important goal during the design of the current collection and transmission systems for high speed trains. One possible method for achieving this goal is the application of an active controller on the pantograph which could improve the contact quality and help achieve longer operation cycles. The active control of the pantograph is realized by allocating a control actuator between the pan-head and the plunger of the pantograph. The goal of this control strategy is to reduce the standard deviation value of the contact force without affecting its mean value. Because the resulting dynamical model of the problem at hand is highly nonlinear, the design of a viable control strategy is a challenging task. Therefore, in the design of an effective controller, the *adjoint method* of optimal control theory seemed appropriate from a mathematical viewpoint whereas the virtual passive control method seemed appropriate from the physical point of view.[8-9] Inspired by both methods, a control action featuring a combined feed-forward plus feedback architecture was designed in order to improve the contact quality in both the transient phase and in the steady state phase of the pantograph/catenary interaction. In particular, the control strategy adopted in this investigation features a derivative structure for the control action integrated with three types of time-varying laws for the controller damping characteristics. In this paper, this particular type of control strategy featuring a feedback plus feed-forward architecture is referred to as *dynamic damping control*. The performance of the designed controller is evaluated by comparing the mean and the standard deviation values of the contact force with and without the controller applied to the system. Numerical simulations showed that the application of the designed controllers on the nonlinear pantograph/catenary system produced a significant improvement in the contact quality. Finally, the robustness of the proposed controllers was

assessed by testing the designed controllers at greater uplift forces. Even in the case of a different uplift force, numerical simulations showed that the proposed control strategies significantly improved the contact quality between the pantograph pan-head and the catenary wire, thus validating the effectiveness of the proposed controllers and widening the scope of their application to various high speed rail infrastructures.

In addition to the control strategy proposed in this investigation, a new method for modeling the pantograph/catenary interaction is proposed. Unlike the method proposed by Seo et al.[5] which requires the use of three gradient vectors when fully parameterized ANCF finite elements are used to model the pantograph/catenary interaction, the new method proposed in this investigation requires the use of only one gradient vector to form a frame at the point of contact between the pan-head and the catenary. Therefore, the proposed new method can be used with both gradient-deficient and fully parameterized ANCF finite elements. The formulation of the contact conditions in terms of one gradient vector is presented. The new approach presented in this paper for modeling the pantograph/catenary interaction can be used with the augmented constraint contact formulation, the embedding constraint contact formulation, or a penalty-based elastic contact formulation. In this investigation, the new formulation is used with the embedding constraint contact formulation in order to demonstrate how the arc length parameter (non-generalized coordinate) can be systematically eliminated using the algebraic contact conditions. The steps for eliminating the arc length parameter at the position, velocity, and acceleration levels are outlined, and it is shown how the arc length parameter and its first and second time derivatives can be expressed in terms of the pan-head and catenary generalized coordinates and their first and second time derivatives.

Because the new sliding joint formulation, which is one of the main contributions of the paper, does not require the use of a complete set of gradients, efficient continuum-based catenary models can be developed and integrated with detailed vehicle model. This formulation is based on a new kinematical description that allows using low order finite elements to obtain a more efficient solution for the pantograph/catenary interaction. As reported in the literature, the constraint and elastic contact formulations, if implemented correctly, give the same nominal values of the forces because the elastic contact can be considered as a penalty approach for imposing the same conditions. For the control study conducted by the authors, the focus is on controlling the nominal value of the contact force, and therefore, the constraint approach is more suited because it filters out high frequency oscillations resulting from the use of the penalty approach. Because the focus of the paper is on controlling the nominal value of the contact force, both approaches should lead to the same conclusions. It is also important to point out that the vehicle dynamics can have a significant effect on the pantograph/catenary interaction. The computational efficiency, however, is more influenced by the high frequencies in the system. Increasing the number of rigid body degrees of freedom does not have the same adverse effect as increasing the frequencies which force the integrator to take a very small time step. The high frequencies in the model used in this paper are mostly attributed to the finite element catenary model, which is also a nonlinear model that requires numerical integration. Therefore, reducing the level of vehicle details will not be of significant help in improving the efficiency. It is important to mention that that the continuum-based catenary model used in this investigation does not employ a modal or linear approach to model the catenary forces. Furthermore, having a detailed coupled analysis is always a step forward toward developing more accurate models.

MBS pantograph/catenary model

In this section, the MBS pantograph/catenary model used in this investigation is described. The approach presented in this investigation is general and can be applied to different railroad vehicle models, including detailed vehicle models in which the wheel/rail contact is described using a three-dimensional contact formulation.

MBS pantograph model

The pantograph system used in this investigation was developed to represent a Faiveley Transport CX pantograph.[7] A general MBS model is employed to describe the pantograph which is assumed to consist of six rigid bodies connected to the car body of the rail vehicle, as shown in Figure 1. The data for the bodies, including the masses, inertial properties, global initial positions, and initial orientations expressed in terms of Euler angles, are given in Table 1. The local reference frame for each body is located at the center of mass and oriented such that the orientation of the axes is defined to be aligned with the principal inertia directions of each body. The kinematic constraints used in this study are described in Table 2, where eight standard joints are used to constrain the motion of the pantograph. The contact between the pantograph head and the catenary is described using a sliding joint.

MBS rail vehicle model

The full rail vehicle model used in this investigation and shown in Figure 2 consists of fourteen rigid bodies, forty-eight bushing elements, eight bearing elements, and two revolute joints. A three-dimensional wheel/rail contact, described later in this section, is used. All bodies of the vehicle model are assumed to be rigid. The data for the vehicle model are provided in Table 3.

The vehicle consists of the car body and two bogies; each bogie includes six bodies, two wheelsets (front and rear), two equalizers (left and right), a frame, and a bolster. This vehicle model includes fifty six force elements, including forty eight bushings and eight bearings. The bushing elements connect the equalizers to the frame and the frame to the bolsters, while the bearings are used to connect the wheelsets to the equalizers. Each of the bolsters is attached to the car body using a revolute joint.

Catenary system

The function of the catenary system is to provide electrical power to the train. The catenary is modeled as a flexible body because of its geometric and material properties. The wire that provides the pantograph with electrical power is called the contact wire. A catenary contact wire typically has a cross-sectional area of roughly 65-150 mm^2 and a span of 50-65 m and is composed of a copper alloy.[10] Based on the type of trains operating on the catenary system, the contact wire may carry between 1,000-25,000 V of power along its length. In addition to the contact wire, in its most basic and simplified configuration, the catenary system consists of a messenger wire, droppers, and support poles as shown in Figure 3. The messenger wire supports the contact wire through droppers between the support poles. The droppers are located between the messenger and contact wires; their purpose is to keep the contact wire parallel to the ground by preventing it from assuming curved shapes. This ensures that power is consistently delivered to the pantograph pan-head. The droppers are usually composed of a copper alloy and carry tension only, that is, they have virtually zero stiffness in compression. The support poles provide support to both the messenger and contact wires at their respective ends. The contact wire is constantly under tension which is the result of the use of tensioning devices and mechanisms.

The tension reduces the sag of the contact wire under its own weight and increases the wave propagation speed, which helps maintain continuous contact with the pantograph pan-head. The tension in catenary systems varies based on the operating speed of the train in the rail corridor. Additionally, the catenary contact wire is supported by registration arms at the support poles which can move horizontally in order to accommodate the longitudinal oscillations of the contact wire.[5] The interaction of the catenary contact wire with the pantograph pan-head causes wear to both the wire itself and more crucially to the pan-head. This wear can be caused by both contact friction and electrical arcing. The electrical arcing occurs when there is a loss of contact between the pan-head and the contact wire, which can inflict very heavy damage on both bodies. More importantly, the loss of contact translates to loss of power to the train. Control systems that help reduce the fluctuations in the contact forces between the pan-head and the contact wire can be used in order to improve the pantograph/catenary system operation, as is shown in this investigation.

ANCF finite element analysis

When excited by an external force arising from the contact with the pantograph, the contact wire undergoes large and non-linear deformation which needs to be modeled accurately in order to realistically simulate the dynamics of the entire system. Several methods have been used in order to model the contact wire, including the Euler-Bernoulli beam, the Fourier sine expansion method, the ANCF cable element, and the ANCF fully parameterized beam element.[6,11-13] There has been a significant amount of research invested in modeling and improving the dynamics of the catenary system because its design affects the operational speed of the train. The contact with the pantograph introduces external forces into the catenary system which creates transverse

waves through the contact wire that have a certain propagation speed. The train speed cannot exceed the catenary wave propagation speed for safety reasons, and the wave reflection effects must also be taken into account in the design of the catenary as well as the operation of the train.[14] In order to include the non-linear large deformation effects, the ANCF cable element was selected to model the catenary contact wire and the messenger wire in this investigation. The ANCF cable element utilizes global position and slope coordinates to define the element displacement field.[15,16] In the ANCF kinematics, the global position vector $\mathbf{r}(\mathbf{x},t)$ of an arbitrary point P on the flexible body is defined as $\mathbf{r}(\mathbf{x},t)=\mathbf{S}(\mathbf{x})\mathbf{e}(t)$, where $\mathbf{x}=[x \quad y \quad z]^T$ is the vector of the element spatial coordinates, t is time, $\mathbf{S}=\mathbf{S}(\mathbf{x})$ is the matrix of element shape functions, and $\mathbf{e}=\mathbf{e}(t)$ is the vector of the element nodal positions and slopes. For an element j on the flexible catenary modeled with cable elements, the vector of the nodal coordinates $\mathbf{e}^j=\mathbf{e}^j(t)$ is defined as follows:

$$\mathbf{e}^{jk}=\left[\mathbf{r}^{jk} \quad \left(\mathbf{r}_x^{jk}\right)^T\right]^T \quad , \quad k=1,2 \tag{1}$$

where k refers to the element node number, $\mathbf{e}^j=\left[\left(\mathbf{e}^{j1}\right)^T \quad \left(\mathbf{e}^{j2}\right)^T\right]^T$ is the vector of the element coordinates, $\mathbf{r}^j=\mathbf{r}^j(\mathbf{x},t)$ is the global position vector of the node j, and $\mathbf{r}_x^j=\mathbf{r}_x^j(\mathbf{x},t)$ represents the element gradient at the respective node j. Advantages of using the ANCF method to analyze large deformations in highly flexible bodies include a constant mass matrix, zero Coriolis and centrifugal effects, and guaranteed continuity of slopes and rotations at the nodal points. Additionally, ANCF finite elements capture a higher number of deformation modes compared to other finite element formulations which only capture selected or specified modes and frequencies.

Catenary ANCF finite element model

The catenary model used in this investigation is based on a simple and basic catenary configuration, which consists of support poles, a messenger wire, droppers, and the contact wire. Assumptions which did not drastically alter the dynamics of the system were applied to the catenary model; examples include the dropper elements being modeled as spring-damper elements which represented the stiffness and damping characteristics of a physical dropper. Additionally, in this work, the staggering of the messenger wire and of the contact wire has been neglected for simplicity. The contact wire was modeled using the three-dimensional ANCF cable element with the material properties of copper. The messenger wire was also modeled using the three-dimensional ANCF cable element and the entire catenary system was represented by a total of 20 spans, where each span is 56.25 m long. The catenary model is showed in the Figure 4 and is described in Table 4. Furthermore, the tensioning of the contact wire as well as the messenger wire is very important in modeling the dynamics of the catenary system. In the finite element model described in this investigation, instead of directly applying nodal forces at the ends of the contact and messenger wires, equivalent nodal displacements are applied to all the nodes that coincide with the support pole positions in order to obtain a suitable pre-tensioning of the catenary. The magnitudes of the displacement boundary conditions applied to the catenary system are calculated based on the tensioning required in the contact and messenger wires, which is 20000 N and 14000 N respectively. A preliminary simulation is performed to compute the stable equilibrium configuration of the catenary system. Using the equilibrium configuration from the initial pre-strained straight configuration of the contact and messenger wires, a separate

set of dynamic simulations are performed with the pantograph and the complete train vehicle model in order to tune the parameters of the proposed control strategies.

The catenary model developed in this paper does not neglect the dropper stiffness in the case of tension. At each time instant, the state of every dropper is individually checked for tension or compression in order to determine its tension or compression state. For simplicity, the slackening of the droppers is neglected in this investigation. Nonetheless, this nonlinear slacking effect can be a topic for future studies.

Pantograph/catenary contact kinematics

Two approaches can be used to model the pantograph/catenary contact, the constraint and elastic contact approaches.[17] The constraint approach will be used in this study in order to avoid the oscillations and high frequencies that result when the elastic contact approach is used. This is particularly important when embarking on a new control investigation as the one considered in this paper. To this end, a sliding joint formulation that requires the use of the concept of the non-generalized coordinates is used.

The sliding joint is used to describe the movement of one body along another when the two bodies are rigid or flexible. Specifically, the sliding joint can be used to model the relative motion between the rigid pan-head of the pantograph and the flexible catenary cable.[5] To this end, considering a contact point P, the constraint equations $\mathbf{C}^s = \mathbf{C}^s(\mathbf{q}^p, \mathbf{e}^c, s, t)$ which represent the sliding joint can be expressed as $\mathbf{C}^s = \mathbf{r}^p - \mathbf{r}^c = \mathbf{0}$ where $\mathbf{r}^p = \mathbf{r}^p(\mathbf{q}^p, t)$ is the global position vector of the contact point P on the pan-head, $\mathbf{r}^c = \mathbf{r}^c(\mathbf{e}^c, s, t)$ is the global position vector of the contact point P on the catenary, $\mathbf{q}^p = \mathbf{q}^p(t)$ is the vector of generalized coordinates of the

pantograph, $\mathbf{e}^c = \mathbf{e}^c(t)$ is the vector of the nodal coordinates of the catenary, and $s = s(t)$ is the non-generalized coordinate which identifies the location of the contact point on the catenary cable. An alternate formulation of the sliding joint constraint equations which employs the unit vectors of a tangent frame defined on the catenary cable is the following:

$$\mathbf{C}^s = \begin{bmatrix} \left(\mathbf{i}_t^c\right)^T \left(\mathbf{r}^p - \mathbf{r}^c\right) \\ \left(\mathbf{j}_t^c\right)^T \left(\mathbf{r}^p - \mathbf{r}^c\right) \\ \left(\mathbf{k}_t^c\right)^T \left(\mathbf{r}^P - \mathbf{r}^c\right) \end{bmatrix} = \mathbf{0} \tag{2}$$

where $\mathbf{i}_t^c = \mathbf{i}_t^c(\mathbf{e}^c, s, t)$, $\mathbf{j}_t^c = \mathbf{j}_t^c(\mathbf{e}^c, s, t)$ and $\mathbf{k}_t^c = \mathbf{k}_t^c(\mathbf{e}^c, s, t)$ are the three unit vectors of a tangent frame defined on the catenary cable at the contact point.[18] In this investigation, a new definition of a contact frame that employs only one gradient vector instead of three gradient vectors is proposed. This allows for developing a general sliding joint formulation that can be used with both ANCF fully parameterized and gradient deficient finite elements. The resulting set of the constraint equations models the pantograph/catenary interaction and it can be used to develop two general approaches to solve the contact problem; the augmented and embedding techniques. The first approach employs the constraint equations and Lagrange multipliers, while in the second approach, the arc length parameter is eliminated to reduce the number of constraint equations to two. In this investigation, the embedding technique is used. The new sliding joint formulation which requires the use of one gradient vector only to define the contact frame and the procedure used to systematically eliminate the arc length parameter are introduced in later sections of this paper.

Wheel/rail contact kinematics

In this study, the assumption of a non-conformal wheel/rail contact is made. The location of the wheel/rail contact points are determined online by solving a set of nonlinear algebraic equations. The solution of these nonlinear equations defines the wheel and rail surface parameters. The four algebraic equations $\left(\mathbf{t}_1^r\right)^T\left(\mathbf{r}^w-\mathbf{r}^r\right)=\mathbf{0},\ \left(\mathbf{t}_2^r\right)^T\left(\mathbf{r}^w-\mathbf{r}^r\right)=\mathbf{0},\ \left(\mathbf{t}_1^w\right)^T\mathbf{n}^r=\mathbf{0}$, and $\left(\mathbf{t}_2^w\right)^T\mathbf{n}^r=\mathbf{0}$, where superscripts w and r refer, respectively, to wheel and rail, $\mathbf{r}^w$ and $\mathbf{r}^r$ are the global position vectors of the potential contact point on the wheel and rail, respectively, $\mathbf{t}_1^w$ and $\mathbf{t}_2^w$ are the tangents to the wheel surface at the contact point, $\mathbf{n}^w$ is the normal to the wheel surface at the contact point, $\mathbf{t}_1^r$ and $\mathbf{t}_2^r$ are the two tangents to the rail, and $\mathbf{n}^r$ is the normal to the rail. The solution of the nonlinear algebraic equations ensures that the contact points on the wheel surface and on the rail surface have the same coordinates along the two tangents $\mathbf{t}_1^r$ and $\mathbf{t}_2^r$, and the tangent planes at the contact point are the same for the two surfaces. These equations can be written in a vector form as $\mathbf{C}^{w,r}\left(\mathbf{q}^r,\mathbf{q}^w,\mathbf{s}^r,\mathbf{s}^w,t\right)=\mathbf{0}$, where $\mathbf{q}^r$ is the vector of generalized coordinates of the rail, $\mathbf{q}^w$ is the vector of generalized coordinates of the wheel, $\mathbf{s}^r$ is the vector of non-generalized coordinates or surface parameters of the rail, $\mathbf{s}^w$ is the vector of non-generalized coordinates or surface parameters of the wheel.[17] Given the vectors of the generalized coordinates of the wheel and rail $\mathbf{q}^w$ and $\mathbf{q}^r$, the nonlinear algebraic equations for each wheel and rail contact can be solved for the surface parameters using an iterative Newton-Raphson solution procedure. To this end, the following equation is used in the Newton-Raphson iterations: $\left(\partial\mathbf{C}^{w,r}/\partial\mathbf{s}^w\right)\Delta\mathbf{s}^w+\left(\partial\mathbf{C}^{w,r}/\partial\mathbf{s}^r\right)\Delta\mathbf{s}^r=-\mathbf{C}^{w,r}$, where $\Delta\mathbf{s}^w$ and $\Delta\mathbf{s}^r$ are the Newton differences.[19]

MBS dynamic equations

Consider a general multibody system which consists of rigid bodies, flexible bodies, and very flexible bodies subject to a set of kinematic constraints and external forces. The vector of system generalized coordinates $\mathbf{p}$ can be written as $\mathbf{p}=\begin{bmatrix}\mathbf{q}_r^T & \mathbf{q}_f^T & \mathbf{e}^T & \mathbf{s}^T\end{bmatrix}^T$, where $\mathbf{q}_r$ defines the reference coordinates of the bodies, $\mathbf{q}_f$ defines the vector of the system small deformations when the floating frame of reference (FFR) formulation is used, $\mathbf{e}$ defines the vector of the system large deformations, and $\mathbf{s}$ defines the vector of non-generalized coordinates or surface parameters. While an elastic wheel/rail contact and embedding sliding joint formulations are used in this investigation, the algorithm developed allows for treating surface parameters as non-generalized coordinates when an augmented wheel/rail contact and sliding joint formulations are used. Using an augmented Lagrangian formulation, the system equations of motion can be written using d'Alembert-Lagrange principle as follows:

$$\begin{bmatrix}\mathbf{M}_{rr} & \mathbf{M}_{rf} & \mathbf{O} & \mathbf{O} & \mathbf{C}_{\mathbf{q}_r}^T \\ \mathbf{M}_{fr} & \mathbf{M}_{ff} & \mathbf{O} & \mathbf{O} & \mathbf{C}_{\mathbf{q}_f}^T \\ \mathbf{O} & \mathbf{O} & \mathbf{M}_{ee} & \mathbf{O} & \mathbf{C}_{\mathbf{e}}^T \\ \mathbf{O} & \mathbf{O} & \mathbf{O} & \mathbf{O} & \mathbf{C}_{\mathbf{s}}^T \\ \mathbf{C}_{\mathbf{q}_r} & \mathbf{C}_{\mathbf{q}_f} & \mathbf{C}_{\mathbf{e}} & \mathbf{C}_{\mathbf{s}} & \mathbf{O}\end{bmatrix}\begin{bmatrix}\ddot{\mathbf{q}}_r \\ \ddot{\mathbf{q}}_f \\ \ddot{\mathbf{e}} \\ \ddot{\mathbf{s}} \\ \boldsymbol{\lambda}\end{bmatrix}=\begin{bmatrix}\mathbf{Q}_r \\ \mathbf{Q}_f \\ \mathbf{Q}_e \\ \mathbf{0} \\ \mathbf{Q}_c\end{bmatrix} \tag{3}$$

where $\boldsymbol{\lambda}$ is the vector of Lagrange multipliers, $\mathbf{M}_{rr}$ is the mass matrix associated with the reference motion of the bodies, $\mathbf{M}_{ff}$ is the mass matrix associated with the system small deformation of the bodies modeled using the FFR formulation, $\mathbf{M}_{rf}$ is the mass matrix that defines the dynamic coupling between the reference motion and the small deformations, $\mathbf{M}_{ee}$ is the mass matrix of the ANCF finite elements, $\mathbf{C}_{\mathbf{q}_r}$, $\mathbf{C}_{\mathbf{q}_f}$, and $\mathbf{C}_e$ are the constraint Jacobian matrices associated with the coordinates $\mathbf{q}_r$, $\mathbf{q}_f$, and $\mathbf{e}$, respectively, $\mathbf{Q}_r$, $\mathbf{Q}_f$, and $\mathbf{Q}_e$ are the

generalized forces associated with these coordinates, and $\mathbf{Q}_c$ is a quadratic velocity vector which results from the differentiation of the constraint equations twice with respect to time.[20]

New sliding joint formulation

In this section, a new constraint formulation for the sliding joint is presented. This formulation can be used to model the contact between the pan-head and the catenary. Unlike the formulation used by Seo et al. which is applicable only to fully parameterized ANCF elements[5], the formulation used in this investigation can be used with both fully parameterized and gradient-deficient ANCF finite elements. This will allow for the development of more efficient catenary models as compared to the models that can be developed using the approach presented by Seo et al.. In the approach used by Seo et al., full parameterization is assumed, and three gradient vectors are required to define a tangent frame which depends on and requires the use of the three gradient vectors. In the method proposed in this section, on the other hand, one gradient vector is required.

Constraint formulation

Recall that the three constraint equations used to define the contact between the catenary and the pan-head were defined in the preceding section and can be rewritten as $\left(\mathbf{r}^c - \mathbf{r}^p\right)^T \mathbf{i}_t^c = 0, \left(\mathbf{r}^c - \mathbf{r}^p\right)^T \mathbf{j}_t^c = 0$, and $\left(\mathbf{r}^c - \mathbf{r}^p\right)^T \mathbf{k}_t^c = 0$. In the approach used in this investigation, the use of unit vectors is not necessary, and only one gradient vector, $\mathbf{r}_x^c = \left[\left(\mathbf{r}_x^c\right)_1 \quad \left(\mathbf{r}_x^c\right)_2 \quad \left(\mathbf{r}_x^c\right)_3\right]^T$ is required. In this case, the three unit vectors $\mathbf{i}_t^c, \mathbf{j}_t^c$, and $\mathbf{k}_t^c$ are replaced, respectively, by the three orthogonal vectors[20,21]:

$$\mathbf{r}_x^c = \begin{bmatrix} \left(\mathbf{r}_x^c\right)_1 \\ \left(\mathbf{r}_x^c\right)_2 \\ \left(\mathbf{r}_x^c\right)_3 \end{bmatrix}, \quad \mathbf{n}_1^c = \begin{bmatrix} -\left(\mathbf{r}_x^c\right)_1 \left(\mathbf{r}_x^c\right)_2 \\ \left(\left(\mathbf{r}_x^c\right)_1\right)^2 + \left(\left(\mathbf{r}_x^c\right)_3\right)^2 \\ -\left(\mathbf{r}_x^c\right)_2 \left(\mathbf{r}_x^c\right)_3 \end{bmatrix}, \quad \mathbf{n}_2^c = \begin{bmatrix} -\left(\mathbf{r}_x^c\right)_3 \\ 0 \\ \left(\mathbf{r}_x^c\right)_1 \end{bmatrix} \tag{4}$$

In these equations, $\left(\mathbf{r}_x^c\right)_k$ refers to the kth component of the gradient vector $\mathbf{r}_x^c$. Note that these three orthogonal vectors, which depend only on the gradient vector $\mathbf{r}_x^c$, are always well defined as long as the gradient vector $\mathbf{r}_x^c$ is not parallel to the vector $\begin{bmatrix} 0 & 1 & 0 \end{bmatrix}^T$. In the case of the singular configuration in which $\mathbf{r}_x^c$ is parallel to the vector $\begin{bmatrix} 0 & 1 & 0 \end{bmatrix}^T$, one can always use the following three orthogonal vectors[20,21]:

$$\mathbf{r}_x^c = \begin{bmatrix} 0 \\ \left(\mathbf{r}_x^c\right)_2 \\ 0 \end{bmatrix}, \quad \mathbf{n}_1^c = \begin{bmatrix} -\left(\mathbf{r}_x^c\right)_2 \\ 0 \\ 0 \end{bmatrix}, \quad \mathbf{n}_2^c = \begin{bmatrix} 0 \\ 0 \\ 1 \end{bmatrix} \tag{5}$$

Using the new orthogonal vectors, one can write the constraint equations for the contact between the catenary and pan-head as

$$\mathbf{C}^s = \begin{bmatrix} \left(\mathbf{r}^c - \mathbf{r}^p\right)^T \mathbf{r}_x^c \\ \left(\mathbf{r}^c - \mathbf{r}^p\right)^T \mathbf{n}_1^c \\ \left(\mathbf{r}^c - \mathbf{r}^p\right)^T \mathbf{n}_2^c \end{bmatrix} = \mathbf{0} \tag{6}$$

These three algebraic equations are functions of one gradient vector only. In the case of the pantograph/catenary contact, these equations can be used to determine the arc length s of the catenary centerline at which the contact occurs. Imposing these contact conditions at the position, velocity, and acceleration levels ensures that the pan-head remains in contact with the catenary. The same algebraic equations can also be used as the basis for developing an elastic contact formulation that allows pantograph/catenary separations. When ANCF finite elements

are used to model the catenary, the element spatial coordinate x can always be written in terms of the arc length s, that is $x = x(s)$. Clearly, $\mathbf{r}_x^c$ and $\mathbf{r}_s^c$ are two parallel vectors and they differ by a scalar multiplier. Therefore, any one of these vectors can be used in the formulation of the preceding algebraic contact equations.

For the control study presented in this paper and in order to avoid discontinuities that result from the use of the elastic contact formulation, a constraint contact approach is used. There are two constraint contact formulations that can be developed, the augmented and the embedded constraint contact formulation. In both formulations, the arc length parameter is treated as a *non-generalized coordinate*.[22] In the first approach, the *augmented constraint contact formulation*, the arc length parameter s is kept in the formulation and is treated as a coordinate that can be selected as a degree of freedom. In the second approach, the *embedded constraint contact formulation*, the arc length is systematically eliminated using the first equation $C_e^s = \left(\mathbf{r}^c - \mathbf{r}^p\right)^T \mathbf{r}_x^c = 0$, while the other two equations, referred to as $\mathbf{C}_m^s = \mathbf{0}$, are not eliminated and are combined with the equations of motion using the technique of Lagrange multipliers. The embedded constraint contact formulation is discussed in the following section.

Embedded constraint contact formulation

In this section, the embedded constraint contact formulation of the sliding joint is discussed. It is shown how one of the algebraic constraint equations of the sliding joint is used to systematically eliminate the arc length parameter. The procedure is demonstrated using the three orthogonal vectors of equation (4).

Elimination of the arc length parameter

The first constraint equation, $C_e^s = \left(\mathbf{r}^c - \mathbf{r}^p\right)^T \mathbf{r}_x^c = 0$ can be used to systematically eliminate the arc length s. For a given set of generalized coordinates, this equation can be considered as a nonlinear equation in the arc length parameter s. An iterative Newton-Raphson algorithm can be used to solve for s by iteratively solving the equation $\left(C_e^s\right)_s \Delta s = -C_e^s$, where $\left(C_e^s\right)_s = \partial C_e^s / \partial s$, and Δs is the Newton difference. One can show that $\left(C_e^s\right)_s = \partial C_e^s / \partial s = \left(\partial \mathbf{r}^c / \partial s\right)^T \mathbf{r}_x^c + \mathbf{r}^{cpT}\left(\partial \mathbf{r}_x^c / \partial s\right)$, where $\mathbf{r}^{cp} = \mathbf{r}^c - \mathbf{r}^p$. Because of the simplicity of the geometry of the catenary, the scalar $\left(C_e^s\right)_s = \left(\partial \mathbf{r}^c / \partial s\right)^T \mathbf{r}_x^c + \mathbf{r}^{cpT}\left(\partial \mathbf{r}_x^c / \partial s\right)$ will be different from zero. This condition is necessary in order to be able to systematically eliminate the arc length s.

In order to impose the other two constraints $\mathbf{C}_m^s = \mathbf{0}$ at the position, velocity, and acceleration levels, one must define the Jacobian matrix of these constraints as well as their first and second time-derivatives. The first constraint leads to $\left(C_e^s\right)_{\mathbf{q}} \delta \mathbf{q} + \left(C_e^s\right)_s \delta s = 0$, where $\mathbf{q} = \begin{bmatrix} \mathbf{e}^T & \mathbf{q}^{pT} \end{bmatrix}^T$ is the vector of the generalized coordinates of the pantograph and catenary, $\left(C_e^s\right)_{\mathbf{q}} = \partial C_e^s / \partial \mathbf{q} = \begin{bmatrix} \partial C_e^s / \partial \mathbf{e} & \partial C_e^s / \partial \mathbf{q}^p \end{bmatrix}$ is the Jacobian matrix associated with the vector of generalized coordinates $\mathbf{q}$, and $\left(C_e^s\right)_s = \partial C_e^s / \partial s = \mathbf{r}^{cpT} \mathbf{r}_{xs}^c + \mathbf{r}_x^{cT} \mathbf{r}_s^c$ is the Jacobian matrix associated with the arc length parameter s. Using the assumption of rigid pan-head, one can show that

$$\left(C_e^s\right)_{\mathbf{q}} = \begin{bmatrix} \partial C_e^s / \partial \mathbf{e} & \partial C_e^s / \partial \mathbf{q}^p \end{bmatrix} = \begin{bmatrix} \left(\mathbf{r}^{cp^T} \mathbf{S}_x + \mathbf{r}_x^{cT} \mathbf{S}\right) & -\mathbf{r}_x^{cT} \mathbf{L}^p \end{bmatrix} \tag{7}$$

In this equation, $\mathbf{L}^p = \partial \mathbf{r}^p / \partial \mathbf{q}^p = \left[\partial \mathbf{r}^p / \partial \mathbf{R}^p \quad \partial \mathbf{r}^p / \partial \boldsymbol{\theta}^p \right] = \left[\mathbf{I} \quad -\mathbf{A}^p \tilde{\bar{\mathbf{u}}}^p \bar{\mathbf{G}}^p \right]$, where $\mathbf{I}$ is the 3×3 identity matrix, $\mathbf{q}^p = \left[\mathbf{R}^{pT} \quad \boldsymbol{\theta}^{pT} \right]^T$, $\mathbf{R}^p$ is the vector the defines the global position vector of the origin of the pan-head coordinate system, $\boldsymbol{\theta}^p$ is the set of parameters used to define the orientation of the pan-head coordinate system, $\mathbf{A}^p$ is the transformation matrix that defines the orientation of the pan-head coordinate system, $\tilde{\bar{\mathbf{u}}}^p$ is the skew symmetric matrix associated with the vector $\bar{\mathbf{u}}^p$ that defines the location of the contact point on the pan-head with respect to the pan-head coordinate system, and $\bar{\mathbf{G}}^p$ is the matrix that relates the angular velocity vector $\bar{\boldsymbol{\omega}}^p$ defined in the pan-head coordinate system to the time derivatives of the pan-head orientation coordinates $\dot{\boldsymbol{\theta}}^p$, that is $\bar{\boldsymbol{\omega}}^p = \bar{\mathbf{G}}^p \dot{\boldsymbol{\theta}}^p$. It follows that

$$\delta s = -\left(\frac{\left(C_e^s\right)_{\mathbf{q}}}{\left(C_e^s\right)_s} \right) \delta \mathbf{q}, \quad \dot{s} = -\left(\frac{\left(C_e^s\right)_{\mathbf{q}}}{\left(C_e^s\right)_s} \right) \dot{\mathbf{q}}, \quad \ddot{s} = -\left(\frac{\left(C_e^s\right)_{\mathbf{q}}}{\left(C_e^s\right)_s} \right) \ddot{\mathbf{q}} - \frac{d}{dt}\left(\frac{\left(C_e^s\right)_{\mathbf{q}}}{\left(C_e^s\right)_s} \right) \dot{\mathbf{q}} \tag{8}$$

For example, in the case of a rigid pan-head in contact with the ANCF catenary, one can show that

$$\dot{s} = -\left(\mathbf{r}^{cpT} \mathbf{v}_x^c + \mathbf{v}^{cpT} \mathbf{r}_x^c \right) \Big/ \left(C_e^s\right)_s = -\left(\left(C_e^s\right)_{\mathbf{q}} \dot{\mathbf{q}} \right) \Big/ \left(C_e^s\right)_s \tag{9}$$

where $\mathbf{v}_x^c = \mathbf{S}_x \dot{\mathbf{e}}$, $\mathbf{v}^c = \mathbf{S}\dot{\mathbf{e}}$, $\mathbf{v}^p = \dot{\mathbf{R}}^p + \boldsymbol{\omega}^p \times \mathbf{u}^p$, $\boldsymbol{\omega}^p$ is the vector that defines the absolute angular velocity of the pan-head body coordinate system, $\mathbf{u}^p = \mathbf{A}^p \bar{\mathbf{u}}^p$ is the vector that defines the position of the pan-head contact point with respect to the pan-head coordinate system, and $\mathbf{v}^{cp} = \mathbf{v}^c - \mathbf{v}^p$.

Derivatives of the contact equations

The derivatives of the contact equations can be written in simpler forms by using the following definitions:

$$\left.\begin{aligned}
&\mathbf{a}^p = \ddot{\mathbf{R}}^p + \boldsymbol{\alpha}^p \times \mathbf{u}^p + \boldsymbol{\omega}^p \times \left(\boldsymbol{\omega}^p \times \mathbf{u}^p\right) \\
&\dot{\mathbf{r}}_x^c = d\mathbf{r}_x^c / dt = \mathbf{S}_x \dot{\mathbf{e}} + \mathbf{r}_{xs} \dot{s} \\
&\ddot{\mathbf{r}}_x^c = d^2 \mathbf{r}_x^c / dt^2 = \mathbf{S}_x \ddot{\mathbf{e}} + 2\left(\mathbf{S}_{xs} \dot{\mathbf{e}}\right) \dot{s} + \mathbf{r}_{xss} \dot{s}^2 + \mathbf{r}_{xs} \ddot{s}
\end{aligned}\right\} \tag{10}$$

where $\boldsymbol{\alpha}^p$ is the angular acceleration vector of the pan-head body coordinate system. Using these definitions, one can write

$$\ddot{s} = -\left(\left(C_e^s\right)_{\mathbf{q}} \ddot{\mathbf{q}} + \left(Q_e^s\right)_c\right) \Big/ \left(C_e^s\right)_s \tag{11}$$

In this equation

$$\left(Q_e^s\right)_c = \left(2\dot{\mathbf{r}}^{cpT} \dot{\mathbf{r}}_x^c + \mathbf{r}^{cpT}\left(2\left(\mathbf{S}_{xs}\dot{\mathbf{e}}\right)\dot{s} + \mathbf{r}_{xss}^c \dot{s}^2\right) + \mathbf{r}_x^{cT}\left(2\left(\mathbf{S}_s \dot{\mathbf{e}}\right)\dot{s} + \mathbf{r}_{ss}^c \dot{s}^2 - \mathbf{a}_c^p\right)\right), \tag{12}$$

and $\mathbf{a}_c^p = \boldsymbol{\omega}^p \times \left(\boldsymbol{\omega}^p \times \mathbf{u}^p\right) + \mathbf{A}^p \tilde{\bar{\mathbf{u}}}^p \dot{\bar{\mathbf{G}}}^p \dot{\boldsymbol{\theta}}^p$.

A virtual change in the coordinates leads to $\delta \mathbf{C}_m^s = \left(\mathbf{C}_m^s\right)_{\mathbf{q}} \delta \mathbf{q} + \left(\mathbf{C}_m^s\right)_s \delta s = \mathbf{0}$. Similarly, one can write the constraints at the velocity level as $\dot{\mathbf{C}}_m^s = \left(\mathbf{C}_m^s\right)_{\mathbf{q}} \dot{\mathbf{q}} + \left(\mathbf{C}_m^s\right)_s \dot{s} = \mathbf{0}$. It follows that

$$\left.\begin{aligned}
&\delta \mathbf{C}_m^s = \left(\left(\mathbf{C}_m^s\right)_{\mathbf{q}} - \frac{1}{\left(C_e^s\right)_s}\left(\mathbf{C}_m^s\right)_s \left(C_e^s\right)_{\mathbf{q}}\right) \delta \mathbf{q} = \mathbf{0} \\
&\dot{\mathbf{C}}_m^s = \left(\left(\mathbf{C}_m^s\right)_{\mathbf{q}} - \frac{1}{\left(C_e^s\right)_s}\left(\mathbf{C}_m^s\right)_s \left(C_e^s\right)_{\mathbf{q}}\right) \dot{\mathbf{q}} = \mathbf{0}
\end{aligned}\right\} \tag{13}$$

These equations show that the Jacobian matrix of the constraints $\mathbf{C}_m^s = \mathbf{0}$ must be modified in order to account for the elimination of the arc length parameter s. One can show that

$$
\left.
\begin{aligned}
\left(C_e^s\right)_{\mathbf{q}} &= \left[\left(C_e^s\right)_{\mathbf{e}^c} \quad \left(C_e^s\right)_{\mathbf{q}^p}\right] = \left[\mathbf{r}^{cpT}\left(\frac{\partial \mathbf{r}_x^c}{\partial \mathbf{e}^c}\right) + \mathbf{r}_x^{cT}\left(\frac{\partial \mathbf{r}^c}{\partial \mathbf{e}^c}\right) \quad -\mathbf{r}_x^{cT}\left(\frac{\partial \mathbf{r}^p}{\partial \mathbf{q}^p}\right)\right] \\
\left(\mathbf{C}_m^s\right)_{\mathbf{q}} &= \left[\left(\mathbf{C}_m^s\right)_{\mathbf{e}} \quad \left(\mathbf{C}_m^s\right)_{\mathbf{q}^p}\right] = \begin{bmatrix} \mathbf{r}^{cpT}\left(\frac{\partial \mathbf{n}_1^c}{\partial \mathbf{e}}\right) + \mathbf{n}_1^{cT}\left(\frac{\partial \mathbf{r}^c}{\partial \mathbf{e}}\right) & -\mathbf{n}_1^{cT}\left(\frac{\partial \mathbf{r}^p}{\partial \mathbf{q}^p}\right) \\ \mathbf{r}^{cpT}\left(\frac{\partial \mathbf{n}_2^c}{\partial \mathbf{e}}\right) + \mathbf{n}_2^{cT}\left(\frac{\partial \mathbf{r}^c}{\partial \mathbf{e}}\right) & -\mathbf{n}_2^{cT}\left(\frac{\partial \mathbf{r}^p}{\partial \mathbf{q}^p}\right) \end{bmatrix} \\
\left(\mathbf{C}_m^s\right)_s &= \begin{bmatrix} \left(\partial \mathbf{r}^c/\partial s\right)^T \mathbf{n}_1^c + \mathbf{r}^{cpT}\left(\partial \mathbf{n}_1^c/\partial s\right) \\ \left(\partial \mathbf{r}^c/\partial s\right)^T \mathbf{n}_2^c + \mathbf{r}^{cpT}\left(\partial \mathbf{n}_2^c/\partial s\right) \end{bmatrix}
\end{aligned}
\right\} \tag{14}
$$

One can show that $\partial \mathbf{r}^c/\partial \mathbf{e}$, $\partial \mathbf{r}^c/\partial s$, and $\partial \mathbf{r}_x^c/\partial \mathbf{e}$ can be written in a straight forward manner in terms of the shape function and its derivative as well as $\partial x/\partial s$. It can be shown also that $\partial \mathbf{n}_1^c/\partial \mathbf{e}$ and $\partial \mathbf{n}_2^c/\partial \mathbf{e}$ can be written, respectively, as

$$
\left.
\begin{aligned}
\partial \mathbf{n}_1^c/\partial \mathbf{e} &= \mathbf{H}_1^c\left(\partial \mathbf{r}_x^c/\partial \mathbf{e}\right) \\
\partial \mathbf{n}_1^c/\partial s &= \mathbf{H}_1^c\left(\partial \mathbf{r}_x^c/\partial s\right) \\
\partial \mathbf{n}_2^c/\partial \mathbf{e} &= \mathbf{H}_2^c\left(\partial \mathbf{r}_x^c/\partial \mathbf{e}\right) \\
\partial \mathbf{n}_2^c/\partial s &= \mathbf{H}_2^c\left(\partial \mathbf{r}_x^c/\partial s\right)
\end{aligned}
\right\} \tag{15}
$$

where

$$
\mathbf{H}_1^c = \begin{bmatrix} -\left(\mathbf{r}_x^c\right)_2 & -\left(\mathbf{r}_x^c\right)_1 & 0 \\ 2\left(\mathbf{r}_x^c\right)_1 & 0 & 2\left(\mathbf{r}_x^c\right)_3 \\ 0 & -\left(\mathbf{r}_x^c\right)_3 & -\left(\mathbf{r}_x^c\right)_2 \end{bmatrix}, \quad \mathbf{H}_2^c = \begin{bmatrix} 0 & 0 & -1 \\ 0 & 0 & 0 \\ 1 & 0 & 0 \end{bmatrix} \tag{16}
$$

While the constraint equations at the acceleration level, $\ddot{\mathbf{C}}_m^s = \mathbf{0}$, can always be obtained by direct differentiation of the constraint equations at the velocity level, a simple approach can be used to define the second derivatives of the constraint functions. Consider a constraint in the

form $\mathbf{r}^{cpT}\mathbf{n}_i^c = \mathbf{0},\ i = 1,2$. The second derivative of this constraint with respect to time can be written as

$$\mathbf{n}_i^{cT}\ddot{\mathbf{r}}^{cp} + 2\dot{\mathbf{r}}^{cpT}\dot{\mathbf{n}}_i^c + \mathbf{r}^{cpT}\ddot{\mathbf{n}}_i^c = \mathbf{0} \tag{17}$$

In this equation,

$$\left.\begin{aligned}
&\dot{\mathbf{r}}^{cp} = \dot{\mathbf{r}}^c - \dot{\mathbf{r}}^p, \quad \ddot{\mathbf{r}}^{cp} = \ddot{\mathbf{r}}^c - \ddot{\mathbf{r}}^p \\
&\dot{\mathbf{r}}^c = \left(\frac{\partial \mathbf{r}^c}{\partial \mathbf{e}}\right)\dot{\mathbf{e}} + \mathbf{r}_x^c\left(\frac{\partial x}{\partial s}\right)\dot{s} \\
&\dot{\mathbf{r}}^p = \mathbf{v}^p = \dot{\mathbf{R}}^p + \boldsymbol{\omega}^p \times \mathbf{u}^p = \mathbf{L}^p\dot{\mathbf{q}}^p \\
&\dot{\mathbf{n}}_i^c = \frac{d}{dt}\left(\mathbf{H}_i^c\mathbf{r}_x^c\right) = \dot{\mathbf{H}}_i^c\mathbf{r}_x^c + \mathbf{H}_i^c\dot{\mathbf{r}}_x^c \\
&\dot{\mathbf{r}}_x^c = \mathbf{S}\dot{\mathbf{e}} + \mathbf{r}_x^c\left(\frac{\partial x}{\partial s}\right)\dot{s} \\
&\ddot{\mathbf{r}}^c = \mathbf{S}\ddot{\mathbf{e}} + 2\left(\mathbf{S}_s\dot{\mathbf{e}}\right)\dot{s} + \mathbf{r}_{ss}\dot{s}^2 + \mathbf{r}_x\ddot{s} \\
&\ddot{\mathbf{r}}^p = \mathbf{a}^p = \ddot{\mathbf{R}}^p + \boldsymbol{\alpha}^p \times \mathbf{u}^p + \boldsymbol{\omega}^p \times \left(\boldsymbol{\omega}^p \times \mathbf{u}^p\right) \\
&\quad = \mathbf{L}^p\ddot{\mathbf{q}}^p + \dot{\mathbf{L}}^p\dot{\mathbf{q}}^p
\end{aligned}\right\} \tag{18}$$

Using the preceding two equations, and writing $\ddot{s}$ in terms of the generalized accelerations $\ddot{\mathbf{q}}$ as explained previously in this section, one can show that the constraint equations at the acceleration level $\ddot{\mathbf{C}}_m^s = \mathbf{0}$ can be written as

$$\ddot{\mathbf{C}}_m^s = \left(\left(\mathbf{C}_m^s\right)_{\mathbf{q}} - \frac{\left(\mathbf{C}_m^s\right)_s\left(C_e^s\right)_{\mathbf{q}}}{\left(C_e^s\right)_s}\right)\ddot{\mathbf{q}} - \left(\mathbf{Q}_m^s\right)_c = \mathbf{0} \tag{19}$$

where $\left(\mathbf{Q}_m^s\right)_c$ is a vector that is quadratic in the velocities. The two scalar equations in equation (19) can be combined with the equations of motion and other constraint equations using the technique of Lagrange multipliers, as previously described in this paper.

Pantograph/catenary contact regulations

The contact between the pan-head and the catenary is defined by a specific European Norm EN50367. The most important parameters used to evaluate the quality of the electrical contact are the mean contact force, the standard deviation in the contact force, and the maximum contact force. The regulations that describe the allowable limits for the contact between the pan-head and the catenary are as follows; Mean Contact Force: $F_m = 0.00097v^2 + 70\,\mathrm{N}$, where v represents the velocity of the train; Standard Deviation: $\sigma_{max} < 0.3F_m$; Maximum Contact Force: $F_{max} < 350\,\mathrm{N}$; Maximum Catenary Wire Uplift at Steady Arm: $d_{up} \le 120\,\mathrm{mm}$; Maximum Pantograph Vertical Amplitude: $\Delta_z \le 80\,\mathrm{mm}$; Percentage of Real Arcing: $NQ \le 0.2\%$. In this investigation, the dynamics of the pantograph catenary computational model were validated using each of the above stated thresholds except the percentage of real arcing.

Adjoint method for optimal control design

In this section, the adjoint method for optimal control design that will be used in this investigation is briefly reviewed. Consider a set of n differential equations which describes the state evolution of a dynamical system as $\dot{\mathbf{z}} = \mathbf{f}$, where $\mathbf{z} = \mathbf{z}(t)$ is the state vector of the dynamical system, $\mathbf{f} = \mathbf{f}(\mathbf{z}, \mathbf{u}, t)$ is the system state function, and $\mathbf{u} = \mathbf{u}(t)$ is the vector of the control actions. Adopting a combination of feedback and feed-forward control strategy, the structure of the control action $\mathbf{u}$ can be pre-established considering a set of time-varying parameters $\boldsymbol{\gamma} = \boldsymbol{\gamma}(t)$ such that $\mathbf{u} = \mathbf{u}(\mathbf{z}, \boldsymbol{\gamma}, t)$. The central idea of optimal control theory is to derive a time history of the control parameters $\boldsymbol{\gamma}$ in order to minimize a cost functional $J = J(\mathbf{z}_0)$, where $\mathbf{z}_0$ is the known system initial state vector. Considering a fixed time domain T for the control actuation, a general form of the cost functional can be expressed as:

$$J = h\big|_T + \int_0^T g dt \tag{20}$$

where $h = h(\mathbf{z}, \tilde{\mathbf{z}}, t)$ is the terminal cost function, $g = g(\mathbf{z}, \tilde{\mathbf{z}}, \mathbf{u}, \tilde{\mathbf{u}}, t)$ is the current cost function, $\tilde{\mathbf{z}} = \tilde{\mathbf{z}}(t)$ is the reference trajectory, and $\tilde{\mathbf{u}} = \tilde{\mathbf{u}}(t)$ is the reference control action. Thus, the problem at hand is to minimize the cost functional J subjected to a set of differential constraint equations which represents the system dynamical model. A method to address the problem under study is to resort to Pontryagin's minimum principle.[23] This algorithm is based on the adjoint method and can be used to obtain the set of differential-algebraic equations whose solution corresponds to the minimum of the cost functional.[24] Therefore, to accomplish this task, the key concept is to exploit the adjoint method which considers the system dynamical model as a set of differential constraint equations for the minimization problem under consideration.[25] To this end, the system state-space equations of motion can be adjoined to the cost functional J to get an augmented cost functional $\bar{J} = \bar{J}(\mathbf{z}_0)$ defined as follows:

$$\bar{J} = h\big|_T + \int_0^T \left(g + \mathbf{v}^T \left(\mathbf{f} - \dot{\mathbf{z}} \right) \right) dt \tag{21}$$

where $\mathbf{v} = \mathbf{v}(t)$ represents a co-state or adjoint state vector which defines the Lagrange multipliers corresponding to the adjoining process of the system dynamical equations to the cost functional J. To simplify the derivation of the necessary conditions which lead to minimum cost functional, a Hamiltonian function $H = H(\mathbf{z}, \tilde{\mathbf{z}}, \mathbf{u}, \tilde{\mathbf{u}}, t)$ can be introduced as $H = g + \mathbf{v}^T \mathbf{f}$. According to Pontryagin's minimum principle, an optimal set of time histories for the system trajectory $\mathbf{z}^* = \mathbf{z}^*(t)$ and for the control parameters $\boldsymbol{\gamma}^* = \boldsymbol{\gamma}^*(t)$ corresponds to a minimum of the Hamiltonian function $H^* = H^*(\mathbf{z}^*, \tilde{\mathbf{z}}, \mathbf{u}^*, \tilde{\mathbf{u}}, t)$. Thus, the augmented cost functional $\bar{J}$ can be

reformulated in terms of the Hamiltonian function H using the integration by parts rule as follows:

$$\bar{J} = h\big|_T + \int_0^T \left(H - \mathbf{v}^T \dot{\mathbf{z}}\right) dt = h\big|_T - \left(\mathbf{v}^T \mathbf{z}\right)\big|_T + \left(\mathbf{v}^T \mathbf{z}\right)\big|_0 + \int_0^T \left(H + \dot{\mathbf{v}}^T \mathbf{z}\right) dt \tag{22}$$

For the problem under consideration, the analytical functions subjected to the minimization procedure are the system state vector $\mathbf{z}$ and the vector of the control parameters $\boldsymbol{\gamma}$. Hence, by using calculus of variation theory,[26] the first variation of the augmented cost functional $\bar{J}$ with respect to the system state vector $\mathbf{z}$ and with respect to the vector of the control parameters $\boldsymbol{\gamma}$ yields:

$$\delta \bar{J} = \left(\left(\left(\frac{\partial h}{\partial \mathbf{z}} \right)^T - \mathbf{v} \right)^T \delta \mathbf{z} \right)\Bigg|_T + \left(\boldsymbol{\lambda}^T \delta \mathbf{z}\right)\big|_0 + \int_0^T \left(\left(\frac{\partial H}{\partial \mathbf{z}} \right)^T + \dot{\mathbf{v}} \right)^T \delta \mathbf{z} + \frac{\partial H}{\partial \boldsymbol{\gamma}} \delta \boldsymbol{\gamma} dt \tag{23}$$

Using the definition of the Hamiltonian function H, the analytic expression of the first variation of the augmented cost functional can be reformulated as:

$$\delta \bar{J} = \left(\left(\boldsymbol{\mu}^T - \mathbf{v} \right)^T \delta \mathbf{z} \right)\Big|_T + \left(\mathbf{v}^T \delta \mathbf{z}\right)\big|_0 + \int_0^T \left(\boldsymbol{\varphi}^T + \mathbf{A}^T \mathbf{v} + \dot{\mathbf{v}} \right)^T \delta \mathbf{z} dt + \int_0^T \left(\boldsymbol{\psi}^T + \mathbf{B}^T \right)^T \delta \boldsymbol{\gamma} dt \tag{24}$$

where $\mathbf{A} = \partial \mathbf{f} / \partial \mathbf{z}$ represents the sensitivity matrix of the system state function $\mathbf{f}$ with respect to the system state $\mathbf{z}$, $\mathbf{B} = \partial \mathbf{f} / \partial \boldsymbol{\gamma}$ represents the sensitivity matrix of the system state function $\mathbf{f}$ with respect to the vector of the control parameter $\boldsymbol{\gamma}$, $\boldsymbol{\mu} = \partial h / \partial \mathbf{z}$ represents the sensitivity vector of the terminal cost function h with respect to the state vector $\mathbf{z}$, $\boldsymbol{\varphi} = \partial g / \partial \mathbf{z}$ represents the sensitivity vector of the current cost function g with respect to the system state $\mathbf{z}$, and $\boldsymbol{\psi} = \partial g / \partial \boldsymbol{\gamma}$ represents the sensitivity vector of the current cost function g with respect to the control parameter vector $\boldsymbol{\gamma}$. Considering that the initial state $\mathbf{z}_0$ is given and assuming that the time domain T is fixed, the necessary conditions which identify the minimum of the cost

functional J can be derived using the fundamental theorem of the calculus of variation to yield:[27]

$$\left.\begin{aligned} &\dot{\mathbf{z}} = \mathbf{f}, \quad \mathbf{z}\big|_0 = \mathbf{z}_0, \quad \dot{\mathbf{v}} = -\left(\boldsymbol{\varphi}^T + \mathbf{A}^T\mathbf{v}\right), \\ &\mathbf{v}\big|_T = \boldsymbol{\mu}\big|_T, \quad \boldsymbol{\psi}^T + \mathbf{B}^T\mathbf{v} = \mathbf{0} \end{aligned}\right\} \tag{25}$$

These resulting differential-algebraic equations constitute a coupled nonlinear two-point boundary value problem which defines the minimum cost functional. The differential-algebraic two-point boundary value problems are challenging to solve analytically but can be solved effectively using certain numerical procedures. For instance, among the gradient-based optimization techniques the iterative adjoint-based control optimization algorithm is an efficient and effective computational method to design control actions for nonlinear mechanical systems.[28-29]

Practical implementation of optimal controller

The suspension used in vehicle dynamic systems can be classified into three categories, each of which could be employed to control the dynamic response of the pantograph. The three categories that can be implemented into the pantograph include passive, semi-active, and active suspension systems. Passive systems have no feedback and thus do not have the ability to filter out undesired frequencies or stabilize a system in response to operative conditions which differ from the desired conditions. These systems also do not have the ability to vary the spring, damping, or actuator forces as a function of time. However, these systems are inexpensive compared to active systems as there are no electronics or measurement devices required. Active controllers, however, are often implemented in dynamic systems to effectively eliminate the undesired motion of the system. The active systems can be implemented via sensor data obtained

from load cells and accelerometers within the system under control. These data are then analyzed in real time by an onboard computer and used to control actuator devices in accordance with the sensor input. This can be costly to implement compared to the passive system because of the additional cost of purchasing and maintaining the input sensors and output devices. Semi-active suspension systems are an attractive alternative to these systems due to the increased performance over the passive system and the decreased economic investment as compared to the active system. These characteristics can be obtained through the use of time-variable dampers which utilize control devices. The smart fluid technology has gained attention for its ability to rapidly change its damping coefficient by changing the fluid properties within the damper from a free-flowing liquid to a semi-solid state. There are two methods in which these smart fluid dampers are controlled: electro-rheological (ER) and magneto-rheological fluids (MR). In ER systems, the fluid within the damper is excited by inducing a large electric field within the damper, whereas the MR systems change the viscosity of the fluid by creating a magnetic field in the damper.[30] MR dampers are able to produce larger dynamic forces and operate at a greater temperature range than ER dampers, and thus MR dampers have drawn more attention from researchers.[31] The MR damper has been studied in a semi-active secondary suspension system on a full-sized railway vehicle as a possible means to control the vertical, pitch, and roll vibrations of the rail vehicle trucks. This system has also been applied to determine if improved ride quality on railway vehicles is feasible and effective.[32] Additionally, MR dampers have been utilized in the seats of commercial vehicles.[33]

Pantograph/catenary contact force

While a detailed MBS vehicle model that includes a flexible pantograph/catenary system is used in this investigation and such a model can be used to determine the pantograph/catenary normal contact forces, in this section a simpler two degree of freedom model is used to obtain an approximation of the nominal value of the contact force. This simpler model, in addition to providing a smoother representation of the normal contact forces, is similar to the models commonly used in the literature. The MBS solution for the contact forces was found to be in a good agreement with the results of the simpler model except for the very high frequencies resulting from the use of the ANCF finite elements.

A simple lumped parameter model of the pan-head/plunger subsystem is developed in this section in order to obtain an estimation of the contact force resulting from the pantograph/catenary interaction. This simple force model will be used to evaluate the controller performance before its application to the more detailed MBS vehicle model that includes the ANCF catenary. A schematic representation of the pan-head/plunger subsystem is shown in Figure 5, where $y_1 = y_1(t)$, $\dot{y}_1 = \dot{y}_1(t)$, and $\ddot{y}_1 = \ddot{y}_1(t)$ are, respectively, the displacement, velocity, and acceleration of the pan-head, $y_2 = y_2(t)$, $\dot{y}_2 = \dot{y}_2(t)$, and $\ddot{y}_2 = \ddot{y}_2(t)$ are, respectively, the displacement, velocity and acceleration of the plunger, m_1 is the mass of the pan-head, m_2 is the mass of the plunger, g is the gravitational acceleration, k_s is the stiffness of the pantograph secondary suspension, l_s is the undeformed length of the secondary suspension, c_s is the damping of the pantograph secondary suspension, $F_c = F_c(t)$ is the contact force between the catenary and the pan-head, and $F_p = F_p(t)$ is the force exerted by the pantograph upper arm. The equations of motion which describe the dynamic behavior of the pan-head/plunger subsystem are the following:

$$\left.\begin{aligned} m_1\ddot{y}_1 &= -k_s\left(\sqrt{(y_1-y_2)^2}-l_s\right)\frac{y_1-y_2}{\sqrt{(y_1-y_2)^2}}-c_s\left(\dot{y}_1-\dot{y}_2\right)-m_1g+F_c \\ m_2\ddot{y}_2 &= -k_s\left(\sqrt{(y_2-y_1)^2}-l_s\right)\frac{y_2-y_1}{\sqrt{(y_2-y_1)^2}}-c_s\left(\dot{y}_2-\dot{y}_1\right)-m_2g+F_p \end{aligned}\right\} \tag{26}$$

Thus, an approximation of the pantograph/catenary interaction force can be computed as

$$F_c = m_1g+m_1\ddot{y}_1+k_s\left(\sqrt{(y_1-y_2)^2}-l_s\right)\frac{y_1-y_2}{\sqrt{(y_1-y_2)^2}}+c_s\left(\dot{y}_1-\dot{y}_2\right) \tag{27}$$

The reduction of the variance in the contact force between the pantograph and the catenary without affecting its mean value is the objective for the design of a control system featuring a feed-forward plus feedback architecture. To this end, the preceding equation for the estimation of the pantograph/catenary interaction force is used to assess the controller performances.

Controllers design and numerical results

In this section, the design of the control system is discussed. Numerical results are also presented in order to demonstrate the effectiveness of the proposed control strategy in improving the behavior of the pantograph/catenary system when complex railroad vehicle models that include significant details are considered. While the new sliding joint formulation proposed in this paper can be used with both gradient deficient and fully parameterized ANCF beam elements, gradient deficient cable elements are used in this investigation to model the catenary in order to have more efficient simulations and avoid some of the locking problems that characterize fully parameterized elements.

Uncontrolled dynamics

The dynamics of an uncontrolled pantograph/catenary system is described in this section. The train is assumed to have a forward speed of 200 km/h and the uplift force applied to the lower arm of the pantograph is assumed to be 1521 N. Because the catenary is limited in length, overlapping transverse waves are generated in the contact wire at the start of the simulation. These waves are gradually attenuated by the dampers between the messenger and the contact wires, and the system reaches a steady state of operation between 1.0 s and 2.0 s. Initially, high frequencies are observed; these represent the waves passing through the system which are attenuated at roughly 1.0 s onwards. Figure 6 shows the variation of the contact force between the pan-head and the contact wire as a function of time. A zoomed window that shows the details of the contact force in the interval between 7.0 s and 10.0 s is presented in Figure 7. The requirements for both the mean contact force and the standard deviation as defined by European Regulation EN50367 are satisfied by the contact force results shown in Figure 6. The mean contact force for an uncontrolled system with an uplift force of 1521 N is -110.427 N, while its standard deviation is 37.3033 N.

Dynamic damping controller design

The goal of the controller design is the reduction of the standard deviation value of the contact force resulting from the pantograph/catenary interaction without affecting its mean value. To this end, the iterative adjoint-based control optimization algorithm is used to obtain the time evolution of the controller parameters for a reduced two dimensional pantograph/catenary model.[8,34-35] This controller is then adapted to the fully non-linear three-dimensional pantograph/catenary model developed in this investigation. In particular, the control strategy adopted features a derivative structure for the control action integrated with three types of time-

varying laws for the controller damping characteristics. The control actuator u is located between the pan-head and the plunger as shown in the following simplified system equations of motion relative to the pan-head/plunger subsystem:

$$\left.\begin{aligned} m_1\ddot{y}_1 &= -k_s\left(\sqrt{(y_1-y_2)^2}-l_s\right)\frac{y_1-y_2}{\sqrt{(y_1-y_2)^2}}-c_s\left(\dot{y}_1-\dot{y}_2\right)-m_1 g+F_c+u \\ m_2\ddot{y}_2 &= -k_s\left(\sqrt{(y_2-y_1)^2}-l_s\right)\frac{y_2-y_1}{\sqrt{(y_2-y_1)^2}}-c_s\left(\dot{y}_2-\dot{y}_1\right)-m_2 g+F_p-u \end{aligned}\right\} \tag{28}$$

The main idea is to design a *dynamic damping controller* by adopting the virtual passive control strategy for tuning the control parameters directly by using the nonlinear model of the pantograph/catenary system. The virtual passive control strategy considers the control system as a passive mechanical subsystem which serves to stabilize the actual dynamical system under study.[9] Thus, the control system is virtual in the sense that it reproduces the dynamics of a mechanical system through the control actions and it is passive because the simulated mechanical system is composed only of passive components. The simplest combination of the virtual passive control strategy with the idea of using a linear dissipative control action yields the derivative control structure $u=-r_c\left(\dot{y}_1-\dot{y}_2\right)$, where $r_c=r_c(t)$ is a damping function which must be designed with a trial-and-error approach using the full nonlinear model. Hence, the derivative controller behaves like a dashpot featuring a damping characteristic r_c which acts in parallel with the physical damper of the secondary suspension c_s. The first control strategy analyzed makes use of a pure feedback architecture featuring a derivative structure with a constant damping coefficient $r_c=r_c^d$. In this investigation, this controller is simply referred to as *derivative controller*. Adopting a purely derivative control strategy, the derivative controller can be simply expressed as $u=-r_c^d\left(\dot{y}_1-\dot{y}_2\right)$, where r_c^d is a constant. An optimal damping coefficient which balances the performance of the contact force in the transient phase and in the steady state phase

was found to be $r_c^d = 3500$ Ns/m, as can be seen in Figure 8. The mean and the standard deviation of the contact force arising from the use of the proposed *derivative controller* are reported in Table 5. The resulting improvement in the contact quality can be quantified considering the relative reduction of the mean and of the standard deviation when comparing the dynamic behavior of the system with and without the *derivative controller* as shown in Table 5. Furthermore, different performances of the *derivative controller* in the transient phase and in the steady state phase of the contact force evolution in time suggest that the value of the controller damping can be adapted to the system behavior using a feedback plus feed-forward control architecture. The simplest method to design a time-varying derivative controller is to use a finite set of damping coefficients which are selected during the time evolution of the nonlinear system, which is the main idea utilized to design a bang-bang controller. Thus, the second control strategy derived in this paper employs a feedback architecture featuring a derivative structure with a time-varying damping coefficient $r_c^{b-b} = r_c^{b-b}(t)$. In this paper, this controller is referred to as *derivative/bang-bang controller*. From a theoretical point of view, it is important to note that a bang-bang controller is the result of an optimal control problem for a nonlinear system featuring a linear control action when a minimum-time response is required and at the same time the control action is limited in magnitude to a prescribed range.[36] Adopting the bang-bang control strategy for the time evolution of the damping, the derivative/ bang-bang control law can be expressed as:

$$u = -r_c^{b-b}\left(\dot{y}_1 - \dot{y}_2\right) \quad , \quad r_c^{b-b} = \begin{cases} r_1^{b-b} & , \quad t < t_c \\ r_2^{b-b} & , \quad t \geq t_c \end{cases} \tag{29}$$

where r_1^{b-b} and r_2^{b-b} are two damping coefficients which must be optimized with a trial-and-error strategy, and t_c is a fixed time instant. An optimal combination of the damping coefficients

found for the dynamical system analyzed in this investigation is $r_1^{b-b} = 1123$ Ns/m and $r_2^{b-b} = 6000$ Ns/m with a time shift at $t_c = 0.5$ s. This combination of damping coefficients considers a trade-off between the contact force behavior in the transient phase and the contact force behavior in the steady-state. The resulting contact force for this *derivative/bang-bang controller* is shown in Figure 9. The mean and the standard deviation of the contact force which arises from the use of the proposed *derivative/bang-bang controller* are reported in Table 5. Moreover, the optimal combination of the damping coefficients for the architecture of the *derivative/bang-bang controller* shows that a small damping magnitude is required in the transient phase whereas a larger damping magnitude is required in the steady state. Thus, the performances of the *derivative/bang-bang controller* suggest that increasing the damping coefficient during the time evolution of the system can further improve the contact quality between the pantograph and the catenary. This idea is used to design the third control strategy considered in this paper which features a simple feedback plus feed-forward *dynamic damping controller* with an exponentially increasing damping coefficient $r_c^e = r_c^e(t)$. In this investigation, this controller is referred to as *derivative/exponential controller*. Therefore, considering an exponential law for the time evolution of the damping, the *derivative/exponential controller* can be expressed as:

$$u = -r_c^e\left(\dot{y}_1 - \dot{y}_2\right) \quad , \quad r_c^e = r_c^f\left(1 - e^{-\frac{t}{\tau_c}}\right) \tag{30}$$

where r_c^f is a constant damping coefficient which arises from the derivative control strategy and τ_c is a time constant which must be optimized with a trial-and-error strategy. In particular, an optimal combination of the damping coefficient and of the time constant which considers a trade-off between the contact force behavior in the transient phase and the contact force behavior in the

steady state is $r_c^f = 7500$ Ns/m and $\tau_c = 0.5$ s. The contact force which results from the implementation of the *derivative/exponential controller* is shown in Figure 10. The mean and the standard deviation of the contact force deriving from the use of the proposed *derivative/exponential controller* are reported in Table 5. These results show that all the designed *dynamic damping controllers* produce a significant improvement in the contact quality between the pantograph pan-head and the catenary wire.

Evaluation of the robustness of the proposed control strategies

From a qualitative point of view, a control system designed assuming a particular set of parameters is robust when it ensures the desired performances for a reasonably wide range of operative conditions which are different from those used to design the controller itself. In order to verify the robustness of the three control strategies proposed, they were tested in a stressed scenario in which a greater value of the uplift force is applied to the lower arm. In particular, an uplift force of 3042 N, which corresponds to an increment of 100% of the nominal uplift force, is considered to perform the robustness test of the proposed controllers and in this investigation this scenario is referred to as high uplift scenario. Considering the high uplift scenario, Figure 11 shows the contact force when the system is uncontrolled, Figure 12 shows a zoomed window of the details of the contact force in the time interval between 7.0 s and 10.0 s, Figure 13 shows the contact force resulting from the application of the *derivative controller*, Figure 14 shows the contact force resulting from the application of the *derivative/bang-bang controller*, and Figure 15 shows the contact force resulting from the application of the *derivative/exponential controller*. In the high uplift scenario, the mean values and the standard deviation values of the contact force arising from the use of respectively all the three types of *dynamic damping*

controllers are shown in Table 6. These results show that the action of the designed derivative controllers on the nonlinear pantograph/catenary system in the high uplift scenario produces a significant improvement in the contact quality characterized by a relative magnitude comparable to that of the design scenario, thus validating the effectiveness of the proposed controllers.

Summary and conclusions

In this investigation, a new sliding joint formulation and a *dynamic damping* control method were developed to control the contact force of the pantograph/catenary system. The new sliding joint formulation requires the use of only one gradient vector, and therefore, it can be used with both ANCF gradient-deficient and fully parameterized beam elements to model the catenary [37-39]. In order to have efficient simulations in this investigation, ANCF cable elements are used to model both the messenger wire and the contact wire. Using this new sliding joint model, three different control strategies were designed to control the contact force between the pantograph and the catenary; these are a *derivative controller*, a *derivative/bang-bang controller*, and a *derivative/exponential controller*. All three proposed controllers improve the standard deviation of the contact force by more than 35% when compared to an uncontrolled system. In order to design an effective controller, accurate modeling of the system dynamics represents a crucial step. The accurate modeling of the pantograph/catenary system was achieved by using ANCF finite elements that can be used in the large deformation and rotation analysis. ANCF finite elements were employed to model the catenary, while a rigid MBS approach was used to model the pantograph and the rail vehicle. Optimal control theory and the theory of virtual passive control were used to design the three different control strategies proposed in this paper. In addition, the robustness of the control strategies was verified by applying the controllers to a

system with a greater uplift force, which is referred to as high uplift scenario. Additionally, the physical implementation of the proposed control laws was discussed, ranging from the use of electro-rheological or magneto-rheological devices to general actuators. It is shown in this investigation that the use of the proposed control method to accurately regulate the contact between the pantograph pan-head and the catenary can be achieved, which can lead to lower wear rates, lower probability of network damage for the rail corridor, and higher interoperability among countries as the behavior of the contact force can be controlled to suit the needs of the region in which the train is operating.

Acknowledgements

This research was supported in part by the U.S. Department of Transportation National University Rail (NURail) Center.

References

1. Bruni S, Bucca G, Collina A, et al. Numerical and Hardware-in-the-Loop Tools for the Design of Very High Speed Pantograph-Catenary Systems. *Journal of Computational and Nonlinear Dynamics*, 2012; 7: 1-8.
2. Bruni S, Facchinetti A. Hardware-in-the-Loop Hybrid Simulation of Pantograph-Catenary Interaction. *Journal of Sound and Vibration*. 2012; 31: 2783-2797.
3. Facchinetti A, Gasparetto L and Bruni S. Real-Time Catenary Models for the Hardware-in-the-Loop Simulation of the Pantograph-Catenary Interaction. *Vehicle System Dynamics: International Journal of Vehicle Mechanics and Mobility*, 2013; 51: 499-516.
4. Poetsch G, Evans J, Meisinger R, et al. Pantograph/Catenary Dynamics and Control. *Vehicle System Dynamics: International Journal of Vehicle Mechanics and Mobility.* 1997; 28: 159-195.
5. Seo JH, Sugiyama H and Shabana AA. Three Dimensional Large Deformation Analysis of the Multibody Pantograph/Catenary Systems. *Journal of Nonlinear Dynamics.* 2005; 42: 199-215.
6. Pombo J and Ambrosio J. Influence of pantograph suspension characteristics on the contact quality with the catenary for high speed trains. *Computers & Structures*. 2012; 110(111): 32-42.
7. Pombo J, Ambrosio J, Pereira M, et al. Influence of the aerodynamic forces on the pantograph-catenary system for high-speed trains. *Vehicle System Dynamics: International Journal of Vehicle Mechanics and Moblity.* 2009; 47(11): 1327-1347.

8. Guida D and Pappalardo CM. A New Method for Control Law Design of a Quarter-Car Suspension System. *International Journal of Mechanical Engineering and Industrial Design*. 2013A; 1(5): 37-58.
9. Juang JN and Phan MQ. *Identification and Control of Mechanical Systems*. Cambridge University Press, Cambridge, 2006.
10. Oura Y, Yoshifumi M and Hiroki N. Railway Electric Power Feeding Systems. *Railway Technology Today*. 2008; 16(3): 48-58.
11. Armbruster K. *Modeling And Dynamics Of Pantograph/Catenary Systems For High Speed Trains*. Thesis, Massachusetts Institute of Technology, USA, 1983.
12. Lee J and Park T. Development of a three dimensional catenary model using cable elements based on absolute nodal coordinate formulation. *Journal of Mechanical Science and Technology*. 2012; 26(12): 3933-3941.
13. Seo JH, Kim S, Jung I, et al. Dynamic analysis of a pantograph-catenary system using absolute nodal coordinates. *Vehicle System Dynamics: International Journal of Vehicle Mechanics and Mobility*. 2006; 44(8): 615-630.
14. Kumaniecka A and Jacek S. Dynamics of the catenarymodelled by a periodical structure. *Journal of Theoretical and Applied Mechanics.* 2008; 46(4): 869-878.
15. Gerstmayr J and Shabana AA. Analysis of Thin Beams and Cables Using the Absolute Nodal Coordinate Formulation. *Journal of Nonlinear Dynamics*. 2006; 45: 109-130.
16. Shabana AA. Computational Continuum Mechanics. 2rd ed, New York: Cambridge University Press, 2012.
17. Shabana AA, Zaazaa KE and Sugiyama H. *Railroad Vehicle Dynamics: A Computational Approach*. Florida: Taylor & Francis/CRC, 2008.

18. Sugiyama H, Escalona JL, Shabana AA. Formulation of Three-Dimensional Joint Constraints Using the Absolute Nodal Coordinates. *Journal of Nonlinear Dynamics*. 2003; 31: 167-195.

19. Shabana AA. Computational Dynamics. 3rd ed, New York: John Wiley and Sons, 2010.

20. Shabana AA. Dynamics of Multibody Systems. 4th ed, Cambridge: Cambridge University Press, 2013.

21. Gere JM and Weaver W. *Analysis of Framed Structures*. D Van Nostrand, New York, 1965.

22. Shabana AA and Sany JR. An Augmented Formulation for Mechanical Systems with Non-Generalized Coordinates: Application to Rigid Body Contact Problems. *Nonlinear Dynamics.* 2001; 24: 183-204.

23. Bryson AE and Ho YC. *Applied Optimal Control: Optimization, Estimation and Control*. Taylor & Francis/CRC, Boca Raton, Florida, USA, 1975.

24. Kirk DE. *Optimal Control Theory: An Introduction.* Dover Publications, 2004.

25. Luchini P and Bottaro A. Adjoint Equations in Stability Analysis. *Annual Review of Fluid Mechanics*. 2014; 46: 1-30.

26. Bewley TR. A Linear Systems Approach to Flow Control. *Annual Review of Fluid Mechanics*, 2007; 39: 383-417.

27. Bewley TR. Flow Control: New Challenges for a New Renaissance. *Progress in Aerospace Sciences*, 2001; 37: 21-58.

28. Guida D and Pappalardo CM. Feed-forward Control Design by Adjoint-Based Control Optimization Method for Hybrid Motion-Force Control of Nonlinear Mechanical Systems. *International Journal of Mechanical Engineering and Industrial Design*. 2014A; Accepted for publication.

29. Guida D and Pappalardo CM. Feedback Control Design by Adjoint-Based Parameter Optimization Method for Hybrid Motion-Force Control of Nonlinear Mechanical Systems. *International Journal of Mechanical Engineering and Industrial Design*. 2014B; Accepted for publication.
30. Jolly MR, Bender JW and Carlson JD. Properties and Applications of Commercial Magnetorheological Fluids. *Smart Structures and Materials 1998: Passive Damping and Isolation*. 1998; 3327: 1-13.
31. Sims ND, Stanway R and Johnson AR. Vibration Control Using Smart Fluids: A State-of-the-Art-Review. *The Shock and Vibration Digest*. 1999; 31(3): 195-203.
32. Liao WH and Wang DH. Semiactive Vibration Control of Train Suspension Systems via Magnetorheological Dampers. *Journal of Intelligent Material Systems and Structures.* 2003; 14(161): 161-172.
33. Choi SB, Nam MH and Lee BK. Vibration Control of a MR Seat Damper for Commercial Vehicles. *Journal of Intelligent Material Systems and Structures*. 2000; 11(936): 936-944.
34. Guida D and Pappalardo CM. Swing-up and Stabilization of an Inverted Pendulum with Dry Friction. *International Journal of Mechanical Engineering and Industrial Design*. 2013B; 2(5): 40-56.
35. Guida D and Pappalardo CM. Development of a Closed-Chain Multibody Model of a High-Speed Railway Pantograph for Hybrid Motion/Force Control of the Pantograph/Catenary Interaction. *International Journal of Mechanical Engineering and Industrial Design*. 2014C; 3(5): 45-85.

36. Juang JN and Phan MQ. Robust Controller Designs for Second-Order Dynamic Systems: A Virtual Passive Approach. *Journal of Guidance, Control, and Dynamics*. 1992; 15(5): 1192-1198.

37. Ren H. A Simple Absolute Nodal Coordinate Formulation for Thin Beams with Large Deformations and Large Rotations. *ASME Journal of Computational and Nonlinear Dynamics.* 2015;10(6):061005-061005-10. doi:10.1115/1.4028610.

38. Shabana A. Definition of ANCF Finite Elements. *ASME Journal of Computational and Nonlinear Dynamics.* 2015;10(5):054506-054506-5. doi:10.1115/1.4030369.

39. Hamper MB, Wei C, and Shabana AA. Use of ANCF Surface Geometry in the Rigid Body Contact Problems: Application to Railroad Vehicle Dynamics. *ASME Journal of Computational and Nonlinear Dynamics.* 2015;10(2):021008-021008-12. doi:10.1115/1.4027442.

Appendix

Notation

$\mathbf{A}$	sensitivity matrix of state function with respect to system state
$\mathbf{B}$	sensitivity matrix of state function with respect to control parameter
$\mathbf{C}$	vector of constraint equations
$\mathbf{C}_{\mathbf{q}_r}$	constraint Jacobian matrix associated with rigid body coordinates
$\mathbf{C}_{\mathbf{q}_f}$	constraint Jacobian matrix associated with FFR body coordinates
$\mathbf{C}_e$	constraint Jacobian matrix associated with ANCF coordinates
c_s	damping value of damper between pan-head and plunger
$\mathbf{e}$	vector of element nodal coordinates of ANCF body
$\mathbf{f}$	system state function
$\bar{\mathbf{G}}^p$	matrix relating the angular velocity vector to the pan-head orientation velocities
g	current cost function
h	terminal cost function
H	Hamiltonian function
J	cost functional
k_s	stiffness of spring between pan-head and plunger
l_s	undeformed length of spring between pan-head and plunger
$\mathbf{L}^p$	Jacobian of position vector of contact point associated with pan-head coordinates
$\mathbf{M}$	mass matrix
m_1	mass of pan-head
m_2	mass of plunger
$\mathbf{n}^w$	normal vector to the wheel surface at the contact point

$\mathbf{n}^r$	normal vector to the rail surface at the contact point
$\mathbf{p}$	vector of system generalized coordinates
$\mathbf{Q}$	vector of system generalized forces
$\mathbf{q}$	vector of generalized coordinates
$\mathbf{r}$	position vector of an arbitrary point
$\mathbf{r}^p$	global position vector of contact point *P* on pan-head
$\mathbf{r}^c$	global position vector of contact point *P* on catenary
r_c^d	damping coefficient of derivative controller
r_c^{b-b}	damping coefficient of derivative/bang-bang controller
r_c^e	damping coefficient of derivative/exponential controller
$\mathbf{S}$	element shape function matrix
s	non-generalized coordinate related to catenary wire
$\mathbf{s}^r$	non-generalized coordinates vector or surface parameters of rail
$\mathbf{s}^w$	non-generalized coordinates vector or surface parameters of wheel
t	time
t_c	time shift constant for derivative/bang-bang controller
$\mathbf{t}^w$	tangent vector to the wheel surface at contact point
$\mathbf{t}^r$	tangent vector to the rail surface at the contact point
$\mathbf{u}$	vector of control actions
$\tilde{\mathbf{u}}$	reference control action
u	control actuator or control force applied to pan-head/plunger subsystem
$\mathbf{v}$	co-state or adjoint vector
$x \quad y \quad z$	element spatial coordinates

y_1, $\dot{y}_1$, $\ddot{y}_1$	position, velocity, acceleration of pan-head
y_2, $\dot{y}_2$, $\ddot{y}_2$	position, velocity, acceleration of plunger
$\mathbf{z}$	state vector of a dynamical system
$\tilde{\mathbf{z}}$	reference trajectory
$\boldsymbol{\omega}$	angular velocity vector
$\boldsymbol{\gamma}$	set of time varying parameters
$\boldsymbol{\mu}$	sensitivity vector of cost function with respect to state vector
$\boldsymbol{\varphi}$	sensitivity vector of the cost function with respect to system state
$\boldsymbol{\psi}$	sensitivity vector of the cost function with respect to vector of control parameters
τ_c	time constant for derivative/exponential controller
$\boldsymbol{\lambda}$	vector of Lagrange multipliers

Table 1. Pantograph body data

Body	**Mass** (kg)	**Initial Position** (m) (x^i_0, y^i_0, z^i_0)	**Initial Orientation** (φ, θ, ψ)	**Inertia** (kg·m^2) (I_{xxi}, I_{yyi}, I_{zzi})
Lower arm	32.18	11.26924156, 0, 3.84511275	$\pi/2$, 0.5528807212, -$\pi/2$	0.31, 10.43, 10.65
Upper arm	15.60	11.45796454, 0, 4.52440451	-$\pi/2$, 0.2896816713, $\pi/2$	0.15, 7.76, 7.86
Lower Link	3.10	10.96436876, 0, 3.81940451	$\pi/2$, 0.6234559506, -$\pi/2$	0.05, 0.46, 0.46
Upper link	1.15	11.58587608, 0, 4.49940451	-$\pi/2$, 0.3028168645, $\pi/2$	0.05, 0.48, 0.48
Plunger	1.51	12.5, 0, 4.835	0, 0, 0	0.07, 0.05, 0.07
Pan-head	9.50	12.5, 0, 4.945	0, 0, 0	1.59, 0.21, 1.78

Table 2. Pantograph joint data

Joint Constraint	**First Body**	**Second Body**
Revolute	Car Body	Lower Arm
Revolute	Lower Arm	Upper Arm
Revolute	Upper Arm	Plunger
Spherical	Car Body	Lower Link
Spherical	Upper Arm	Lower Link
Spherical	Plunger	Upper Link
Spherical	Lower Arm	Upper Link

Table 3. Vehicle body data

Body	**Mass** (kg)	**Inertia** (kg·m^2) (I_{xxi}, I_{yyi}, I_{zzi})	**Initial Position** (m) (x^i_0, y^i_0, z^i_0)
Rail	---	---	---
Wheelsets	2091	1098, 191, 1098	0, 0, 0.4570488
			2.5908, 0, 0.4570488
			12.573, 0, 0.4570488
			15.1638, 0, 0.4570488
Equalizers	469	6.46, 255, 252	1.2954, 1.0287, 0.3049427
			1.2954, -1.0287, 0.3049427
			13.8684, 1.0287, 0.3049427
			13.8684, -1.0287, 0.3049427
Frame	3214	1030, 1054, 2003	1.2954, 0, 0.5081427
			13.8684, 0, 0.5081427
Bolster	1107	498, 20.4, 458	1.2954, 0, 0.7088
			13.8684, 0, 0.7088
Car Body	24170	30000, 687231, 687231	1.8289, 0, 1.8289

Table 4. Catenary properties

Contact/Messenger Wire Geometry	
Elements per Span	9
Element Length (m)	6.25
Element Cross Section Area (mm^2)	144
Total Number of Spans	20
Catenary System Material Properties	
Contact Wire Density (kg/m^3)	8960
Contact Wire Modulus of Elasticity (Pa)	1.2E+11
Messenger Wire Modulus of Elasticity (Pa)	1.2E+11
Other General Catenary Properties	
Tension in Contact Wire (N)	20000
Tension in Messenger Wire (N)	14000
Dropper Stiffness k_d (N/m)	200000
Dropper Damping C_d (N/m)	10000

Table 5. Controller results comparison with low lift

Controller Type	r^1 (Ns/m)	r^2 (Ns/m)	t_c (s)	τ_c (s)	**Mean Force** (N)	**Std. Dev** (N)	**Δ Mean Force**	**Δ Force Std. Dev**
Uncontrolled	/	/	/	/	-110.427	37.3033	/	/
Derivative	3500	/	/	/	-110.241	22.709	-0.169 %	-39.123 %
Bang-Bang	1123	6000	0.5	/	-110.304	21.214	-0.111%	-43.129%
Exponential	7500	/	/	0.5	-110.330	20.800	-0.088%	-44.238%

Table 6. Controller results comparison with high lift

Controller Type	r^1 (Ns/m)	r^2 (Ns/m)	t_c (s)	τ_c (s)	**Mean Force** (N)	**Std. Dev** (N)	**Δ Mean Force**	**Δ Force Std. Dev**
Uncontrolled	/	/	/	/	-468.145	41.688	/	/
Derivative	3500	/	/	/	-468.466	31.478	+0.685 %	-24.490 %
Bang-Bang	1123	6000	0.5	/	-468.653	30.522	-0.108%	-26.783%
Exponential	7500	/	/	0.5	-468.715	30.336	+0.122%	-27.230%

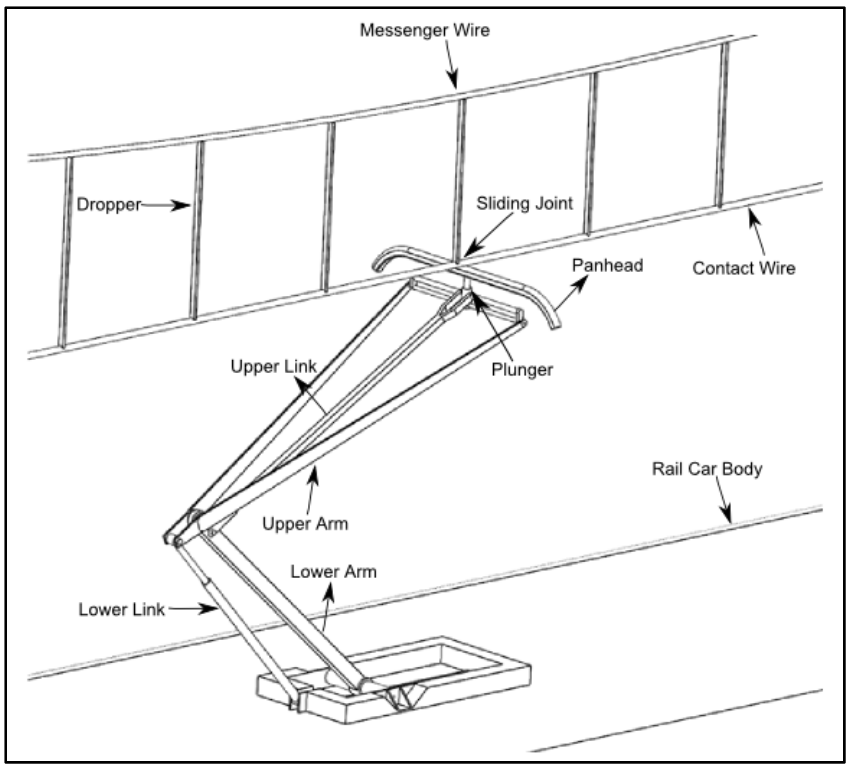

Figure 1. Pantograph and catenary system

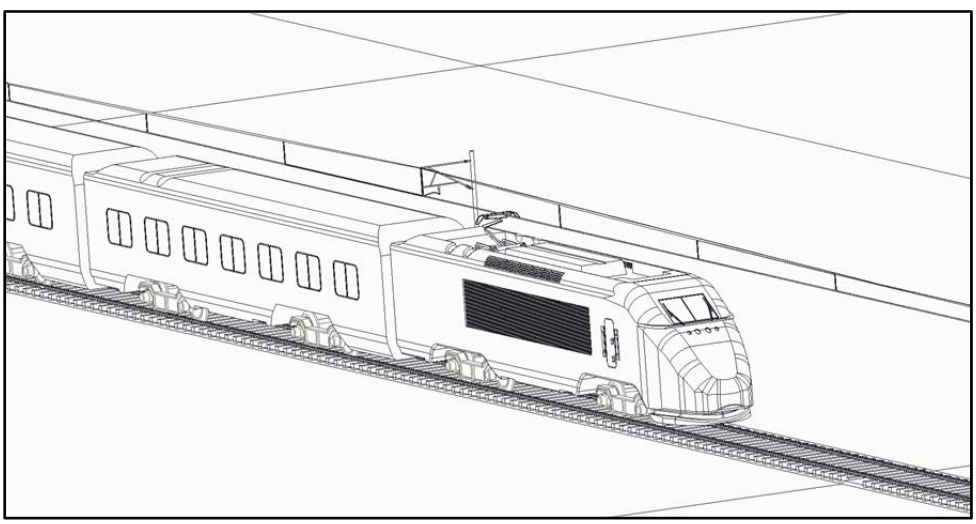

Figure 2. Rail vehicle model

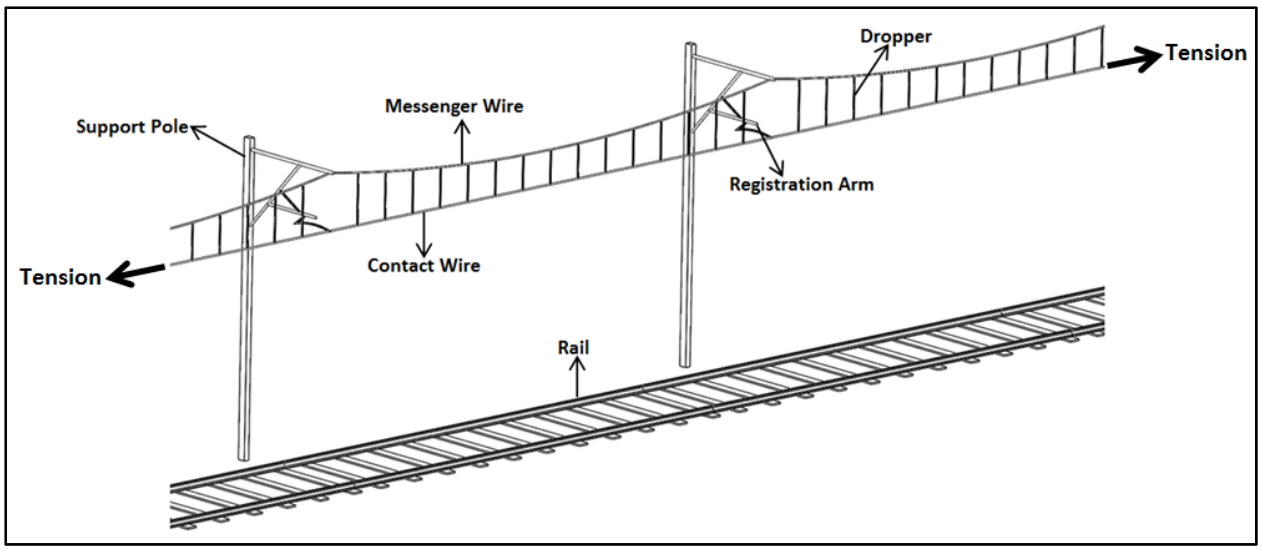

Figure 3. Catenary system

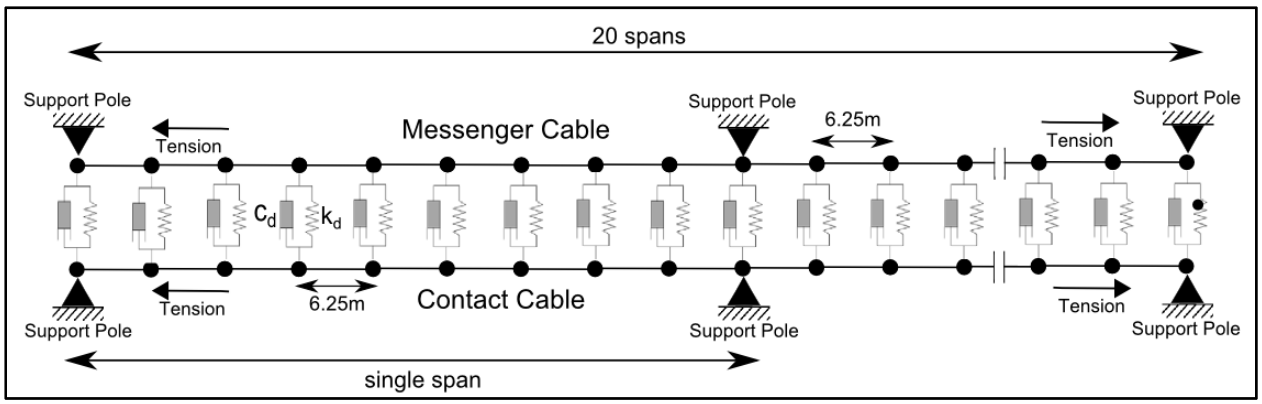

Figure 4. Catenary computational model

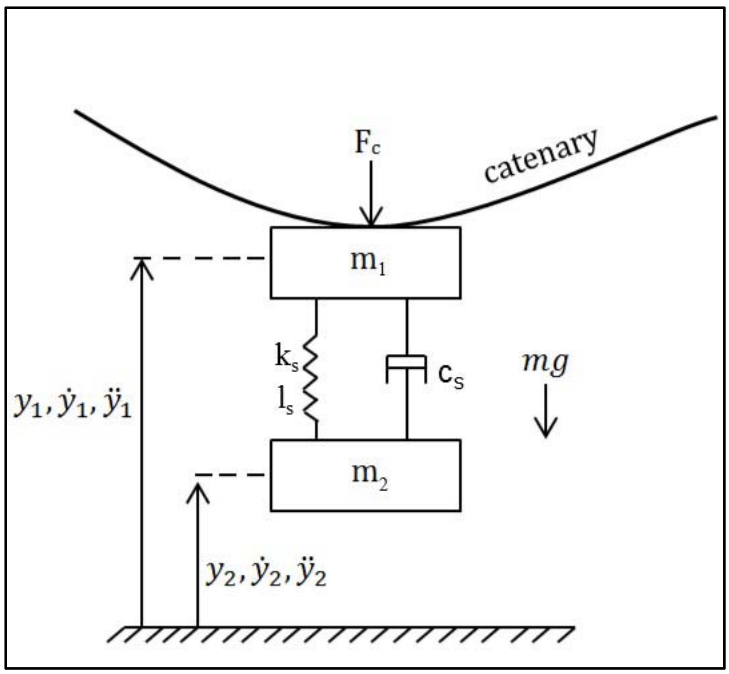

Figure 5. Pan-head/plunger subsystem

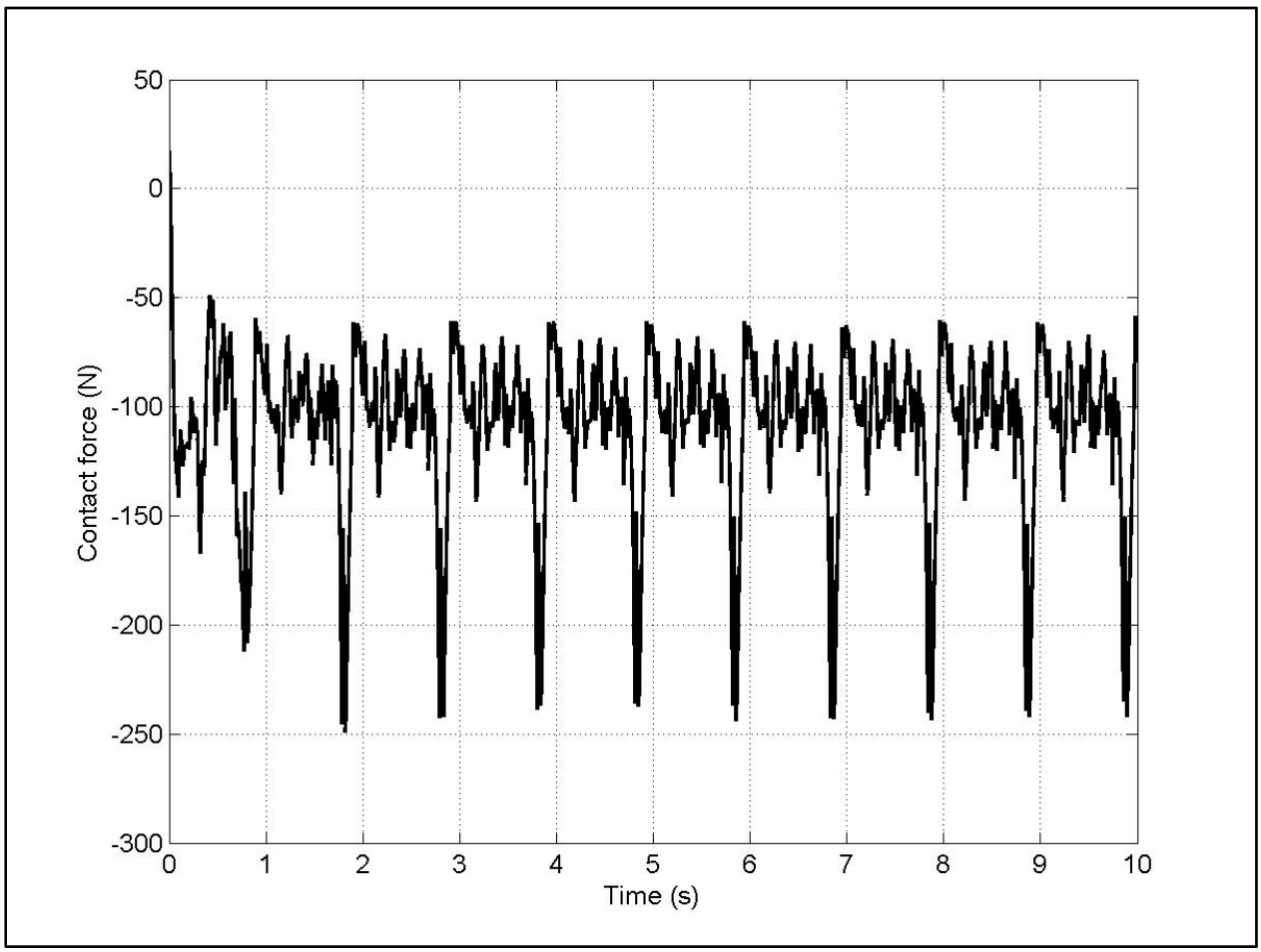

Figure 6. Contact force with low lift (—— no control)

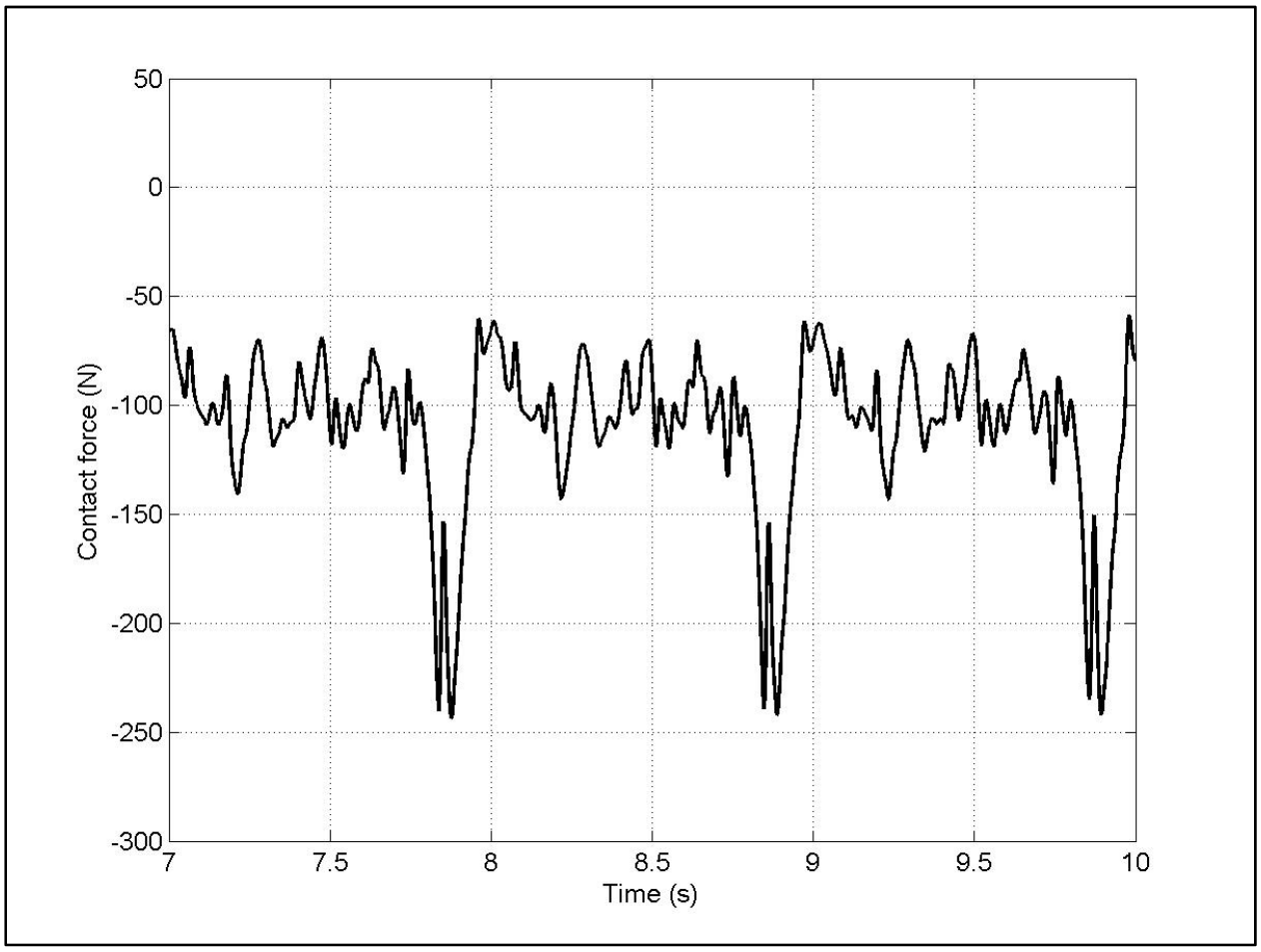

Figure 7. Zoomed window of the contact force with low lift (—— no control)

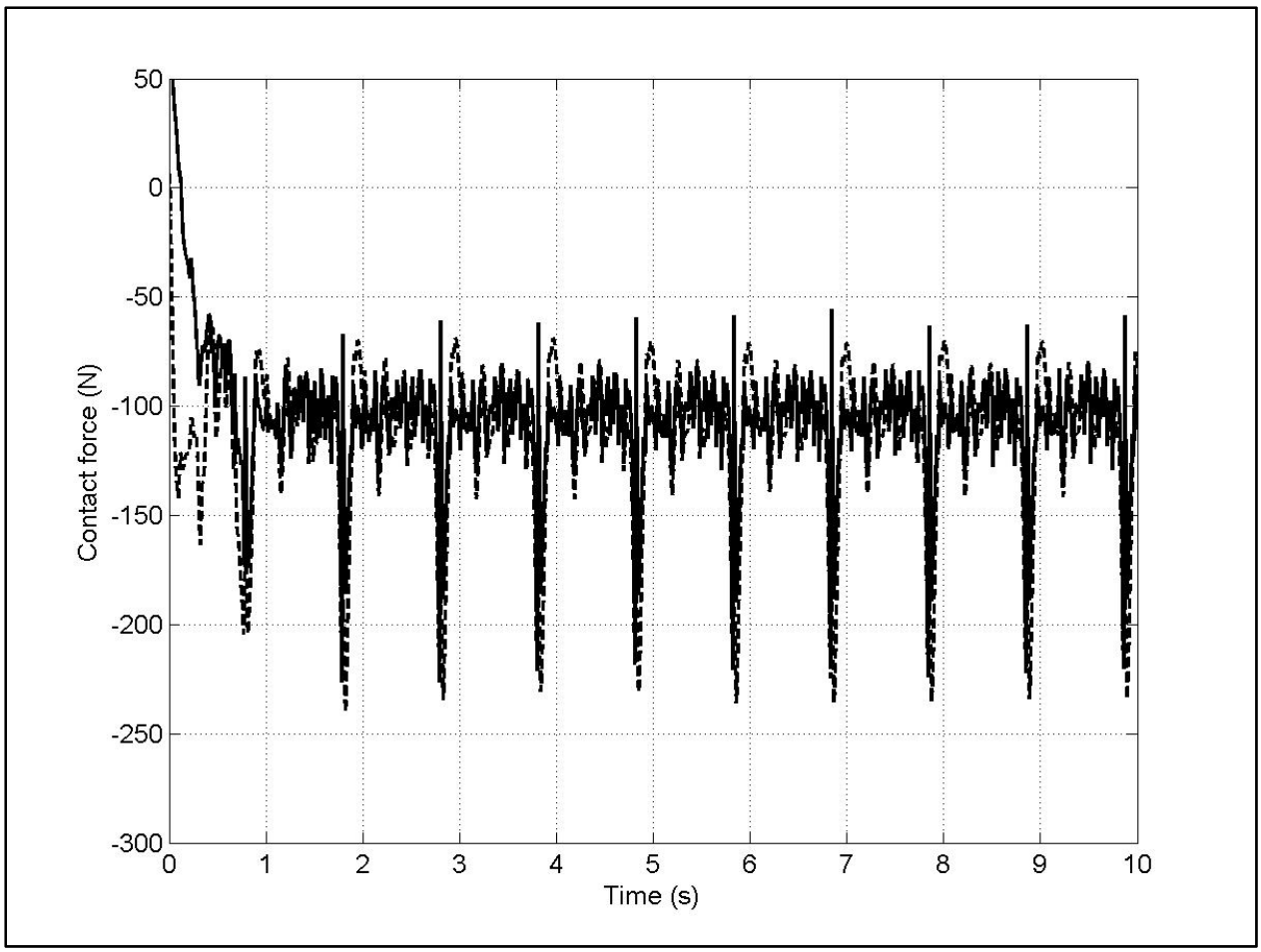

Figure 8. Contact force with low lift (– – – no control, —— derivative control)

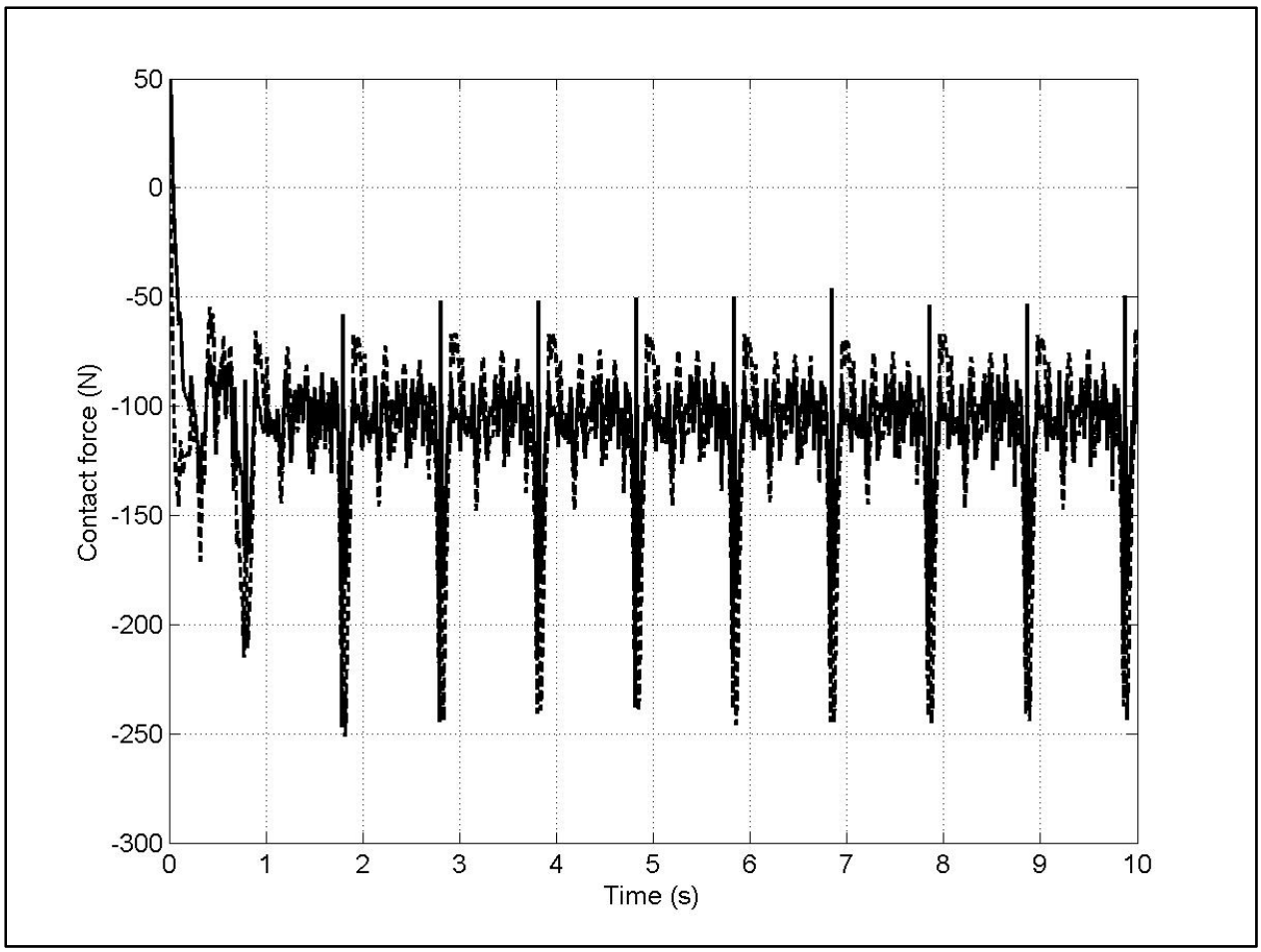

Figure 9. Contact force with low lift (– – – no control, —— derivative/bang-bang control)

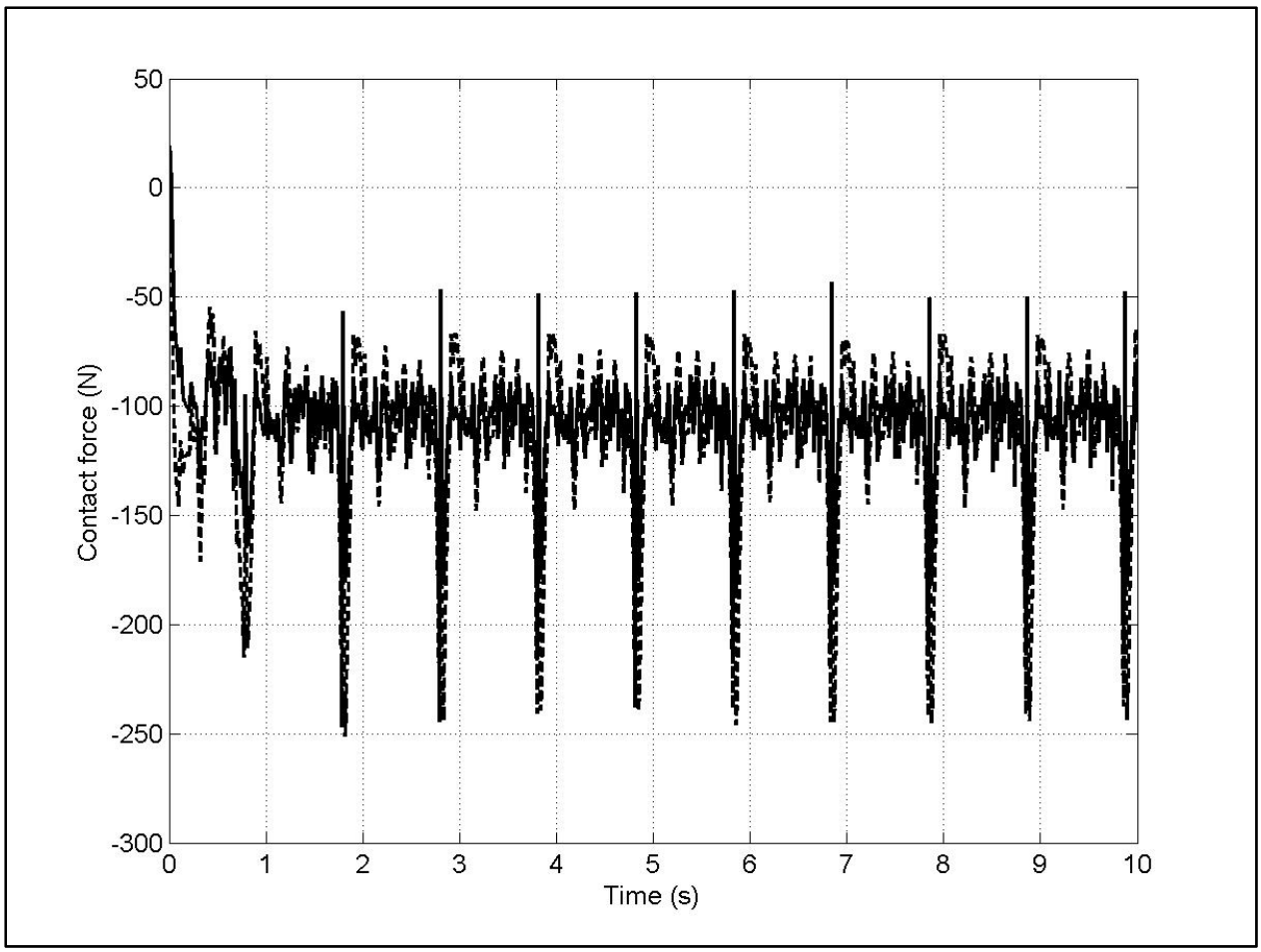

Figure 10. Contact force with low lift (– – – no control, —— derivative/exponential control)

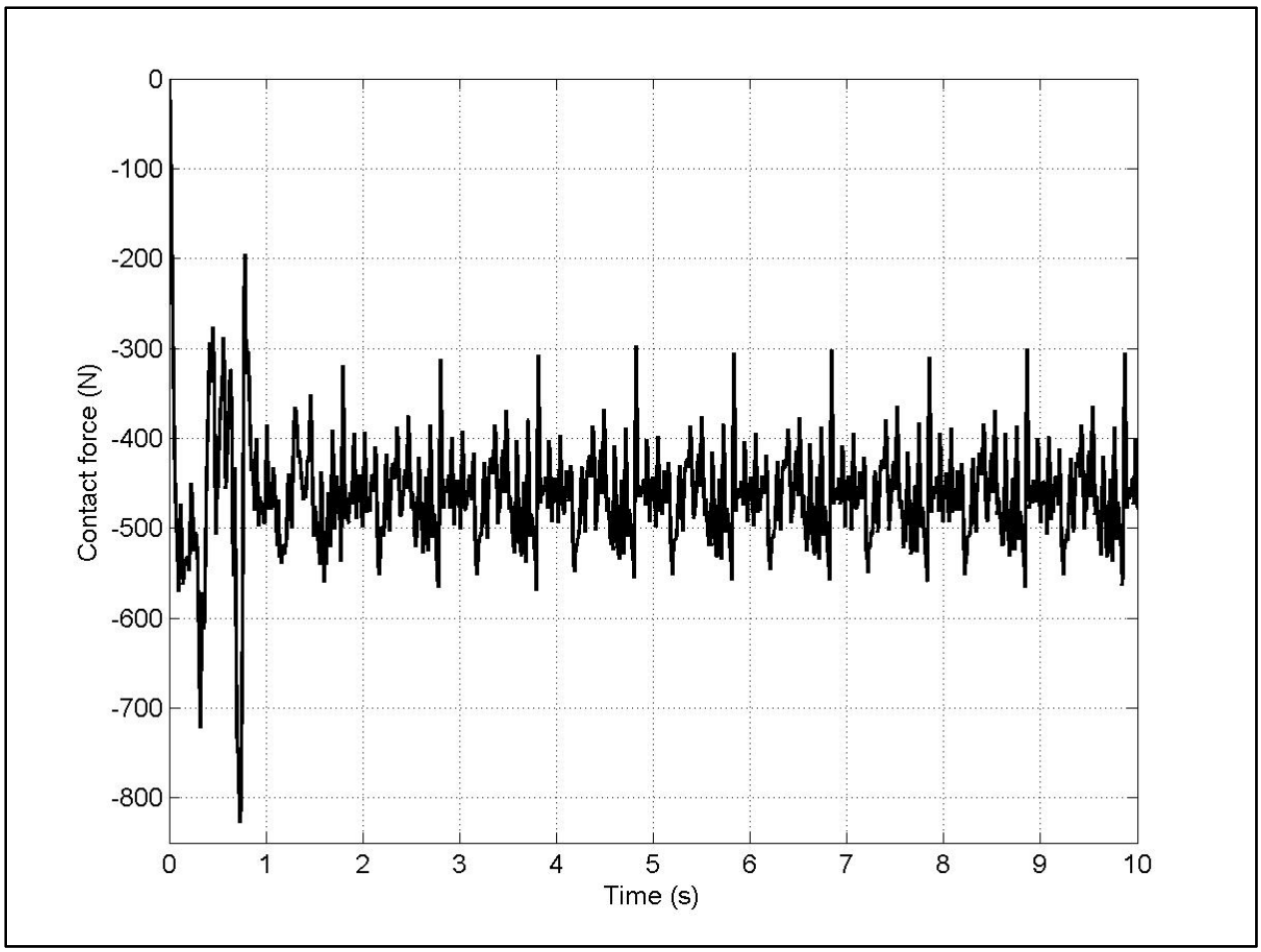

Figure 11. Contact force with high lift (—— no control)

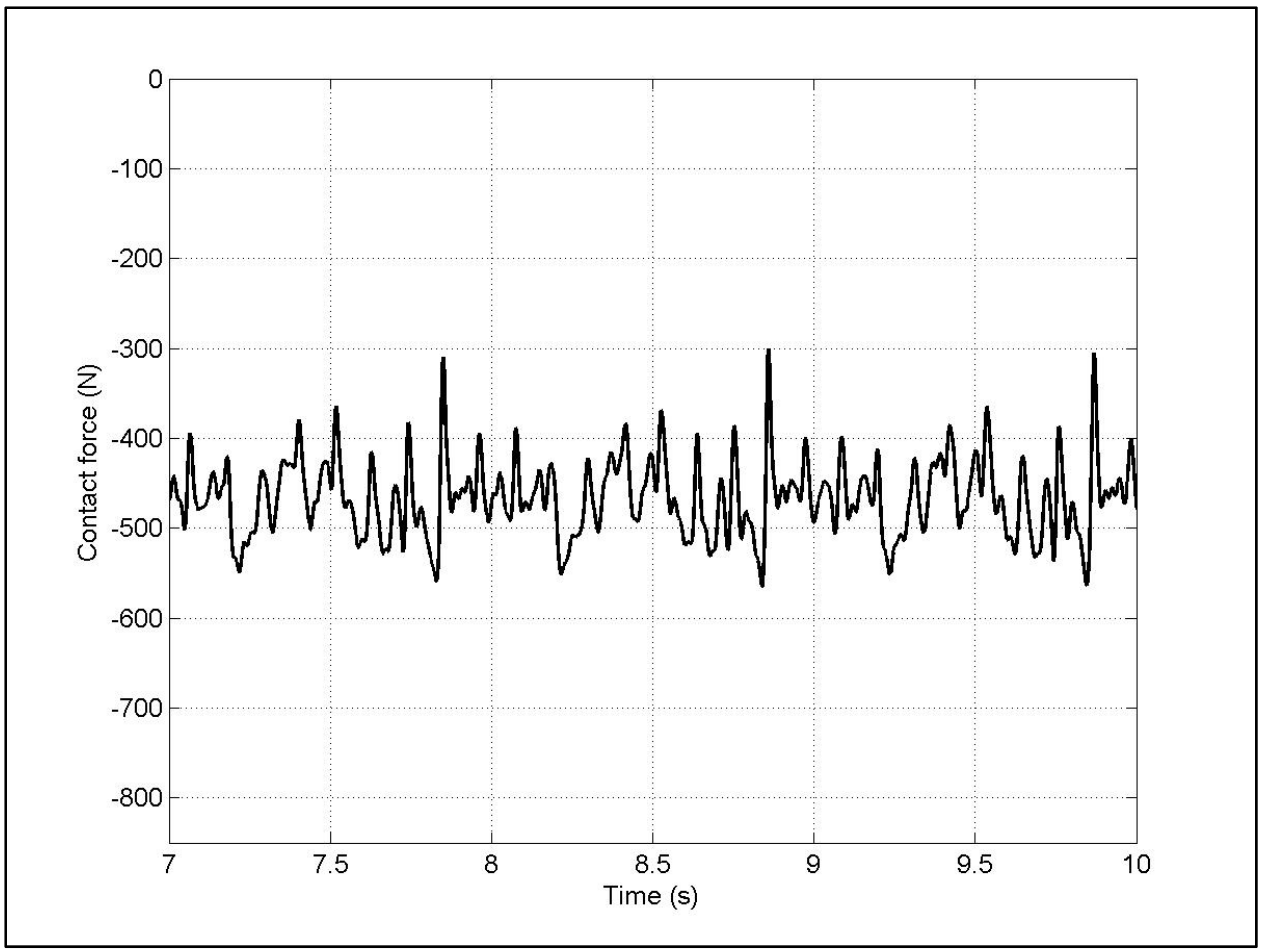

Figure 12. Zoomed window of the contact force with high lift (—— no control)

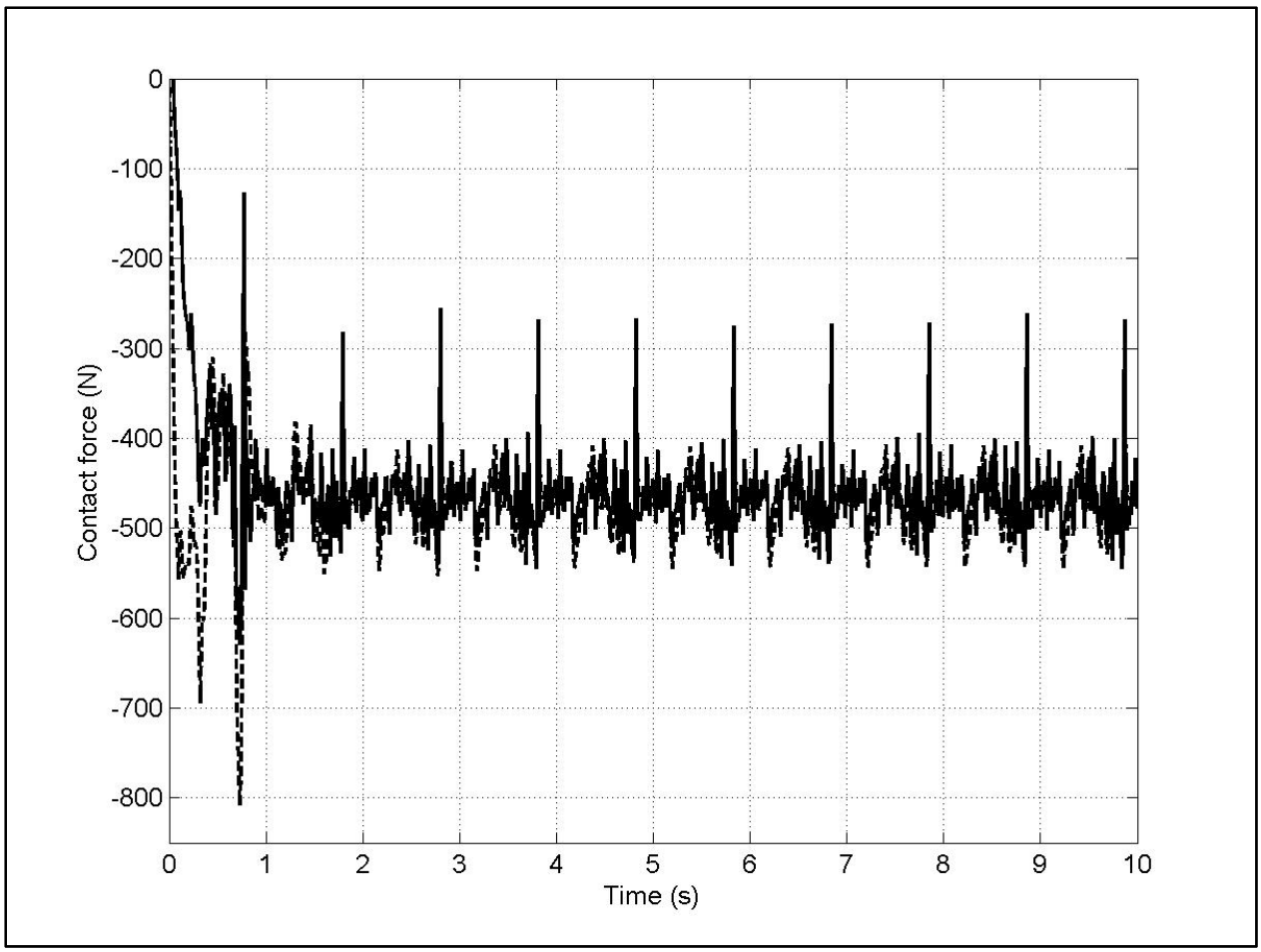

Figure 13. Contact force with high lift (– – – no control, —— derivative control)

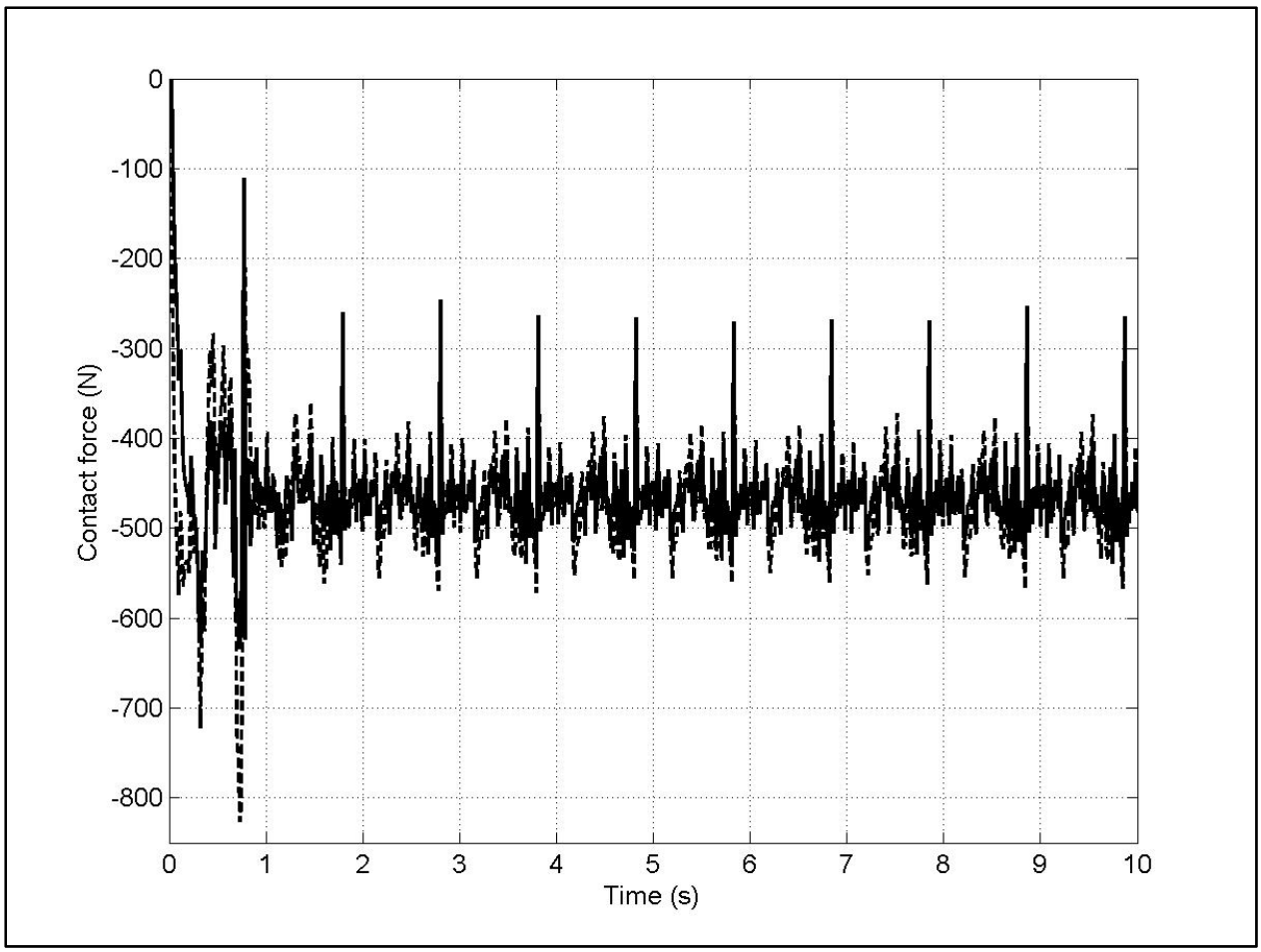

Figure 14. Contact force with high lift (– – – no control, —— derivative/bang-bang control)

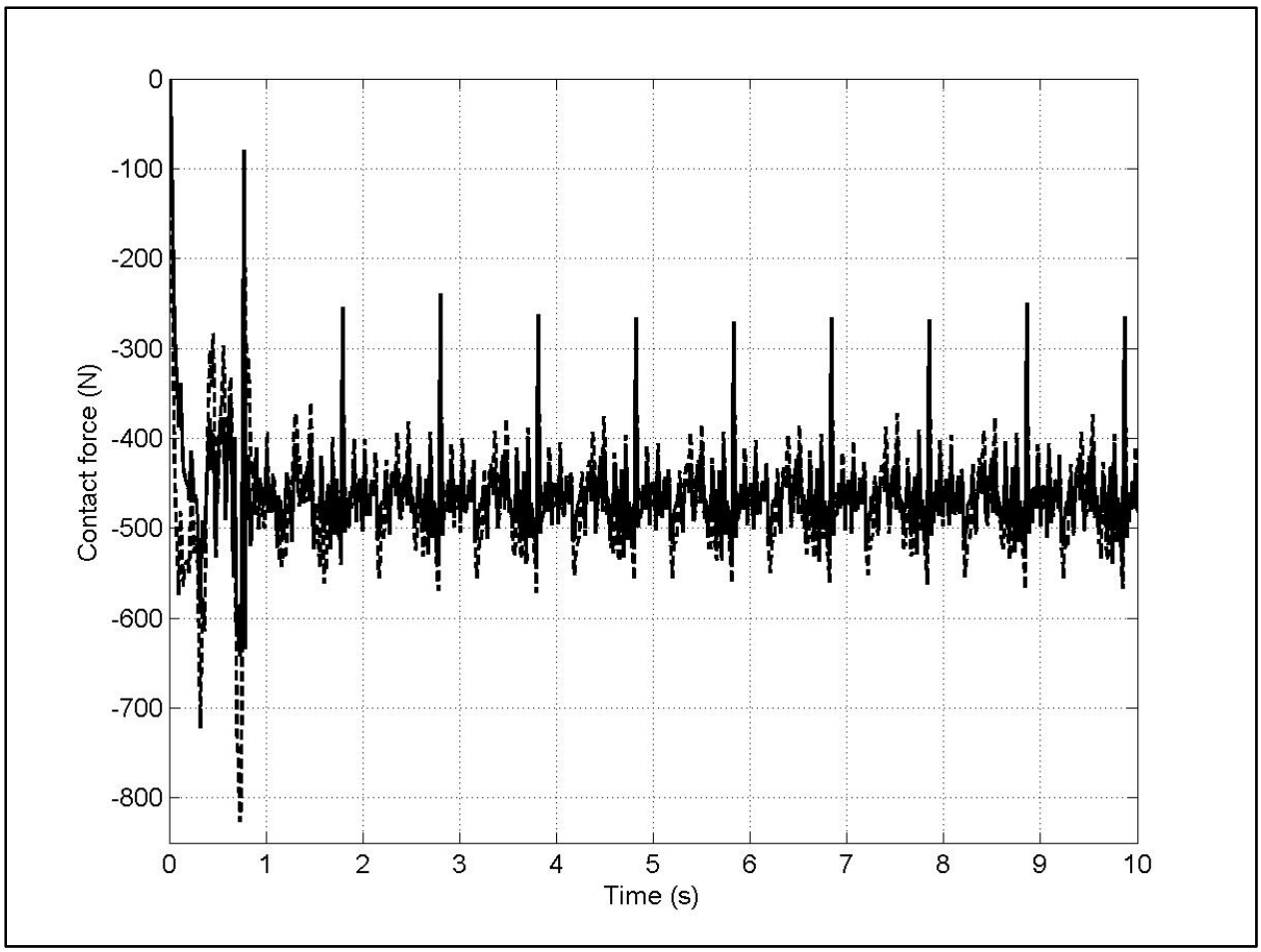

Figure 15. Contact force with high lift (– – – no control, —— derivative/exponential Control)